UNIVERSITY OF SÃO PAULO
INSTITUTE OF ENERGY AND ENVIRONMENT
POSTGRADUATE PROGRAM IN ENERGY

LUANA BATISTA MORAES

Assessment of overvoltages on medium voltage circuits of hybrid overhead lines due to direct lightning strikes

SÃO PAULO
2024

LUANA BATISTA MORAES

Assessment of overvoltages on medium voltage circuits of hybrid overhead lines due to direct lightning strikes

Corrected Version

Dissertation presented to the Postgraduate Program in Energy at the Institute of Energy and Environment of the University of São Paulo to obtain the title of Doctor of Science.

Supervisor:

Prof. Dr. Alexandre Piantini

SÃO PAULO

2024

PUBLISHER'S CATALOGING-IN-PUBLICATION DATA

Batista Moraes, Luana

Assessment of overvoltages on medium voltage circuits of hybrid overhead lines due to direct lightning strikes / Luana Batista Moraes; supervisor Alexandre Piantini – São Paulo, 2024.

82 p.: il; 31 cm.

Ph.D. Dissertation (Doctorate degree in Science) – Postgraduate program in Energy – Institute of Energy and Environment of the University of São Paulo.

1. Overhead hybrid lines 2. Direct strokes 3. Scale model. I. Title

Prepared by Maria Penha Silva Oliveira CRB-8/6961

BATISTA MORAES, L. **Assessment of overvoltages on medium voltage circuits of hybrid overhead lines due to direct lightning strikes.** 2024. Ph.D. Dissertation presented to the Postgraduate Program in Energy at the Institute of Energy and Environment of the University of São Paulo to obtain the title of Doctor of Science.

Approved on: May 10th, 2024

Examination Committee

Prof. Dr. Maria Teresa Correia de Barros
Institution: University of Lisboa
Decision: Approved

Prof. Dr. Carlo Alberto Nucci
Institution: University of Bologna
Decision: Approved

Prof. Dr. Marcos Rubinstein
Institution: University of Applied Sciences of Western Switzerland (HEIG-VD)
Decision: Approved

Prof. Dr. Farhad Rachidi
Institution: Swiss Federal Institute of Technology Lausanne
Decision: Approved

Prof. Dr. Pantelis N. Mikropoulos
Institution: Aristotle University of Thessaloniki
Decision: Approved

ACKNOWLEDGEMENTS

Firstly, I'd like to thank God for the blessed life I have.

I thank my advisor Prof. Dr. Alexandre Piantini for the opportunity to carry out this research and for being the guide throughout its development, in the quest to be as thorough and precise as possible in seeking the intended results. In addition to all the knowledge passed on all these years working together.

I thank my mother Maria Lucília Batista Moraes and my father Silvio de Almeida Moraes who educated me and made me the woman I am today, taught me respect, being fearful of God, Jesus and Mary and passed on to me all the values I carry as a person. I pray to God that my mother, who I miss so much today, is watching over me and my entire family and I thank my father for being so strong that he was the pillar that supported our family at the time of my mother's death.

I would like to thank my colleague Dr. Miltom Shigihara for his friendship and for all his help in the laboratory during the construction of the reduced scale model of the line, the measurements, and tests necessary to complete this work, and for all the conversations and exchanges of experiences during difficult times that comprise any research.

I would like to thank my colleague Maurício for his support in making the towers and insulators of the reduced-scale model of the line, which was essential for collecting measurements in the laboratory and completing this work. I would also like to thank the IEE/USP High Voltage Laboratory for help during the atmospheric impulse tests.

I would like to thank CAPES for the financial support throughout these years of my PhD, which, without it, I would not have been able to continue with my research.

I would like to thank the manufacturer Siklowatt insulators for supplying the 138 kV polymeric insulator. Finally, I would like to thank the Institute of Energy and Environment and the Postgraduate Program in Energy at the University of São Paulo for the opportunity.

“The important thing is not to stop questioning”

Albert Einstein

ABSTRACT

BATISTA MORAES, L. **Assessment of overvoltages on medium voltage circuits of hybrid overhead lines due to direct lightning strikes**. 2024. 82 p. Ph.D. Dissertation – Postgraduate Program in Energy, Universidade de São Paulo, São Paulo, 2024.

The continuous population growth in large cities has become an obstacle in constructing new distribution lines due to the limitations of available space. To address this concern, the construction of hybrid overhead lines, which are overhead lines composed of sub-transmission and distribution circuits, has been seen as a viable solution. However, despite the advantages, few studies have been devoted to the lightning performance analysis of this type of line. This Ph.D. Dissertation analyzes surges caused by direct lightning strokes to a hybrid overhead line composed of 138 kV, 13.8 kV, and 220 V circuits, primarily focusing on the medium voltage (MV) line overvoltages. Specific models for the transmission towers and high-voltage (HV) insulators were validated through tests and simulations. A reduced-scale model of a section of four spans of an actual hybrid overhead line was developed and deployed. Currents were injected at the top of the central tower, and voltages were measured at different points along the tower and on the HV and MV circuits. Comparisons between measured and calculated (using the EMTP) results were performed on this line type for the first time. The deviations between the peak voltages measured and calculated absolute values varied from 1.2% to 16%. The results indicated the adequacy of the models used in the EMTP simulations and in the reduced-scale system. In addition to analyzing the overvoltages on the MV circuit and their dependence on the main parameters, critical currents were also calculated for different combinations of soil resistivity and ground impulse impedance. The analysis confirms the excellent lightning performance of the hybrid overhead line, even for the most challenging conditions considered in the study.

Keywords: direct strokes; distribution lines; electromagnetic transients; hybrid overhead lines; lightning overvoltages; lightning performance, measurements; scale models.

RESUMO

BATISTA MORAES, L. **Avaliação de sobretensões em circuitos de média tensão de linhas aéreas híbridas devido a descargas atmosféricas diretas**. 2024. 82 p. Tese de Doutorado - Programa de Pós-Graduação em Energia da Universidade de São Paulo, São Paulo, 2024.

O contínuo crescimento populacional nas grandes cidades tornou-se um obstáculo na construção de novas linhas de distribuição devido a limitações de espaço disponível. Para responder a esta preocupação, a construção de linhas aéreas híbridas, que são linhas aéreas compostas por circuitos de subtransmissão e distribuição, tem sido vista como uma solução viável. Contudo, apesar das vantagens, poucos estudos têm sido dedicados à análise do desempenho deste tipo de linha frente a descargas atmosféricas. Nesta Tese de Doutorado são analisados os surtos causados por descargas atmosféricas diretas em uma linha aérea híbrida composta por circuitos de 138 kV, 13.8 kV e 220 V, com foco principal nas sobretensões na linha de média tensão (MT). Modelos específicos para torres de transmissão e isoladores de alta tensão (AT) foram validados através de testes e simulações. Um modelo em escala reduzida de uma seção de quatro vãos de uma linha aérea híbrida real foi desenvolvido e implantado. As correntes foram injetadas no topo da torre central e as tensões foram medidas em diferentes pontos ao longo da torre e nos circuitos de AT e MT. Comparações entre resultados medidos e calculados (usando o EMTP) foram realizadas neste tipo de linha pela primeira vez. Os desvios entre os valores absolutos dos valores de pico das tensões medidas e calculadas variaram na faixa de 1.2% a 16%. Os resultados indicaram a adequação dos modelos utilizados nas simulações tanto no EMTP quanto no sistema em escala reduzida. Além de analisar as sobretensões no circuito de MT e sua dependência dos principais parâmetros, também foram calculadas as correntes críticas para diferentes combinações de resistividade do solo e impedância impulsiva do sistema de aterramento. A análise confirma o excelente desempenho da linha aérea híbrida contra descargas atmosféricas, mesmo para as condições mais severas consideradas no estudo.

Palavras-chave: descargas atmosféricas diretas, desempenho frente a descargas atmosféricas, linhas de distribuição, linhas aéreas híbridas, medições, modelo reduzido, sobretensões atmosféricas, transitórios eletromagnéticos.

LIST OF FIGURES

LIST OF TABLES

TABLE OF CONTENTS

1. INTRODUCTION

The continuous population growth in large metropolitan areas has become an obstacle in the plan of new distribution lines, primarily due to the limitations of available space. Consequently, the realization of new projects incurs increased costs. To address this concern, the construction of hybrid overhead lines, which are overhead lines composed of sub-transmission and distribution circuits (as illustrated in Fig. 1), has been seen as a viable solution (NOVITSKIY; WESTERMANN, 2012).

The deployment of hybrid overhead lines holds the potential to reduce costs associated with novel power distribution infrastructure by benefitting from the operational integration of existing sub-transmission lines. However, despite these advantages, few studies have been devoted to the lightning performance analysis of this type of line (e.g. BORGHETTI et al., 2018b, 2019b, 2020).

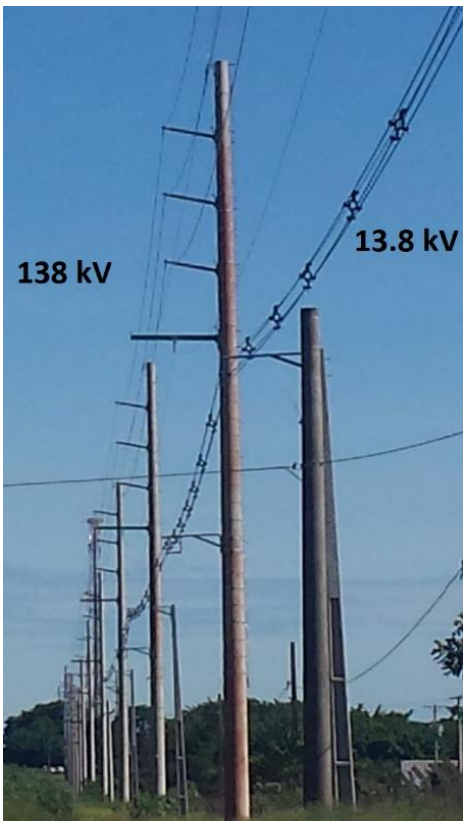

Fig. 1. Hybrid overhead line composed of 138 kV and 13.8 kV circuits (Campo Grande, Brazil), before the installation of the low-voltage circuit. (BATISTA MORAES et al., 2023)

Lightning and switching transients are the primary origins of overvoltages occurrences in both sub-transmission and distribution lines (BATISTA MORAES et al., 2017a). In regions characterized by high or moderate lightning flash densities, power line outages mainly result from lightning events.

In prior research, Rugthaicharoencheep (2012) conducted simulations using the Alternative Transient Program (ATP) to analyze a hybrid overhead line composed of 69 kV and 24 kV circuits affected by direct lightning strokes. Notably, the study showed that overvoltage amplitudes often reach levels capable of causing insulator flashovers in both circuits.

Similarly, MORAES et al. (2017) assessed overvoltage peaks resulting from direct strokes to a hybrid overhead line composed of 69 kV, 13.8 kV, and 220 V circuits. Using the ATP [7], simulations included scenarios where direct strokes hit the top of the central tower, the midpoint of the span, and the highest phase conductor of the high-voltage (HV) line. Examination of overvoltages across line insulators included two distinct lightning current waveforms: a stroke with a magnitude of 80 kA and a 15/107 μs waveform hitting the central tower top and mid-span and a stroke of 34 kA magnitude and a 5/40 μs waveshape on the highest phase of the HV line. While overvoltage amplitudes in the medium-voltage (MV) circuit remained below the line basic insulation level (110 kV), overvoltages in the low-voltage circuit exceeded the withstand voltage level, causing flashovers. Proposed mitigation strategies included the installation of surge protective devices on every tower and pole of the hybrid overhead line.

Further studies, documented by BORGHETTI et al. (2018b, 2019b, 2020), investigated overvoltage scenarios due to direct strokes to two distinct hybrid overhead line configurations: one including 69 kV and 11.4 kV circuits, and the other comprising 138 kV and 13.8 kV circuits. Using the LIOV-EMTP (PGSTECH; POWERSYS, 2023), the investigation entailed a comparison of the lightning performances of the MV circuit of the hybrid line and a conventional MV line, considering both direct and indirect strokes. Additionally, the influence of surge arrester installation at varying spacings along the MV line was evaluated. In (BORGHETTI et al., 2018a, 2019a), the analysis focused on the former configuration of 69 kV and 11.4 kV circuits, assessing flashover occurrences across MV insulators caused by both direct and indirect strokes. The presence of a HV circuit can mitigate overvoltages in the MV circuit. However, a low-voltage (LV) circuit beneath the MV line, if present, can experience induced voltages of substantial magnitude, requiring consideration, especially in regions characterized by significant lightning activity.

Subsequently BATISTA MORAES et al. (2022) validated their EMTP calculations against measurements obtained from a scale model of a hybrid overhead line for the case of direct strokes. Once a reasonable agreement was established, the influences of the stroke current front time, ground resistivity, and ground impedance on the overvoltages in the MV circuit were evaluated through EMTP simulations.

The papers published to date show the importance of studying the behavior and performance of hybrid overhead lines against lightning. By evaluating the effects of direct lightning strikes in this type of construction, it is possible to mitigate their effects, make hybrid overhead lines viable and improve the quality of the electrical system.

The magnitude and waveform of the lightning overvoltages depend on the stroke current, network configuration, and soil characteristics (PIANTINI; BORGHETTI; NUCCI, 2020). Knowing how the main parameters affect the overvoltages is of great importance to evaluate the lightning performance of a hybrid overhead line. In this dissertation, the effects of the main parameters on the lightning overvoltages on MV lines are evaluated.

Unlike the studies published so far about hybrid overhead lines that are based only on results from computer simulations, this thesis also includes measurements carried out in a reduced-scale model of a section of an actual hybrid overhead line. The HV line insulator and the tower models were developed and validated based on comparisons involving tests carried out in the HV and Scale Model laboratories of the Institute of Energy and Environment of the University of São Paulo.

Analyses of hybrid overhead lines are also currently being carried out by the CIGRE Working Group (WG) C4.67 (Lightning Protection of Hybrid Overhead Lines). Its activities started in January 2022 and the main objectives of the WG are to assess the overvoltages caused by direct and indirect strokes on hybrid overhead lines and to analyze the lightning performances of their distribution circuits, making comparisons with conventional distribution circuits alone. It also aims to provide guidelines for the safety of persons and protection of equipment in low-voltage networks supplied by hybrid overhead lines, as well as assess the lightning overvoltages on typical multi-circuit transmission lines with different rated voltages and protection methods. The efforts made by the CIGRE WG highlight the importance and relevance of the study of hybrid overhead lines.

1.1. Objective

The main objective of this research is to analyze lightning overvoltages on a MV line that share the same structure with a HV line and a LV line. The analysis is carried out through computer modeling and simulation of the system under study, as well as laboratory tests using a reduced-scale model of a representative line section. As the shielding failure rate has a marginal impact on the lightning performance of the considered line because of the conductor's heights and positions, the analysis of the effects of direct strikes focuses on the backflashover phenomenon.

The research comprises the following specific goals:

- to develop models for the tower and insulators of an actual hybrid overhead line and validate them experimentally;
- to develop a reduced-scale system for experimental studies of lightning overvoltages on a hybrid overhead line;
- to construct and validate a hybrid overhead line model in the EMTP, through comparisons with measurements performed in the reduced-scale model;
- to evaluate the influence of the most important parameters on the MV line overvoltages;
- to estimate the critical currents (first and subsequent strokes) for the HV and MV circuits of the hybrid overhead line considering different conditions for the soil resistivity and ground impulse impedance.

1.2. Outline of the Dissertation

This Dissertation is organized in six chapters. The first presents an introduction, the objective, and the structure of the Dissertation.

The second chapter presents the models for each line components, with emphasis on the developed models for the tower and 138 kV insulators and their validation through laboratory tests.

The third chapter describes the reduced scale model implemented to simulate a hybrid overhead line and presents comparisons between voltages and currents on the MV line calculated using the EMTP and measurements carried out on scale model.

The fourth chapter evaluates the overvoltages in the MV line and their dependence on key parameters such as the ground impulse impedance, soil resistivity, stroke current front time, conductor characteristics, lightning channel impedance, insulator capacitance, conductors' sag, and tower surge impedance.

In the fifth chapter, an analysis of the lightning performance of the line is carried out where the critical currents are calculated considering different values for the soil resistivity and the ground impulse impedance.

The final chapter presents the main conclusions and contributions of the work, as well as topics for future research.

2. MODELING

The line examined in this study consists of three circuits and a total of 13 conductors. These include an overhead ground wire (OHGW) placed at the top of the structure, a HV (138 kV) circuit, an underbuilt shield wire (USW) positioned 2 m below the lowest phase conductor, a MV circuit employing spacer cable technology with a rated voltage of 13.8 kV, and a LV circuit using a multiplex cable at 220 V. The line configuration is illustrated in Fig. 2 and Fig. 3.

In this dissertation the following definitions, taken from (IEEE, 1997), are used:

- Overhead ground wire (OHGW): grounded wire or wires placed above the phase conductors for the purpose of intercepting direct strokes in order to prevent the phase conductors from the direct strokes;
- Underbuilt shield wire (USW): shield wires arranged among or below the average height of the protected phase conductors for the purposes of lowering the OHGW system impedance and improving coupling.

A total of 22 spans is considered in the simulations (corresponding to the total line length of 1.76 km), with an extended span of 10 km at each line termination. The distance between adjacent towers is 80 m, and an MV pole is located at the center of each span, as shown in Fig. 2.

The forthcoming subsections present a detailed description of the models for the individual system components.

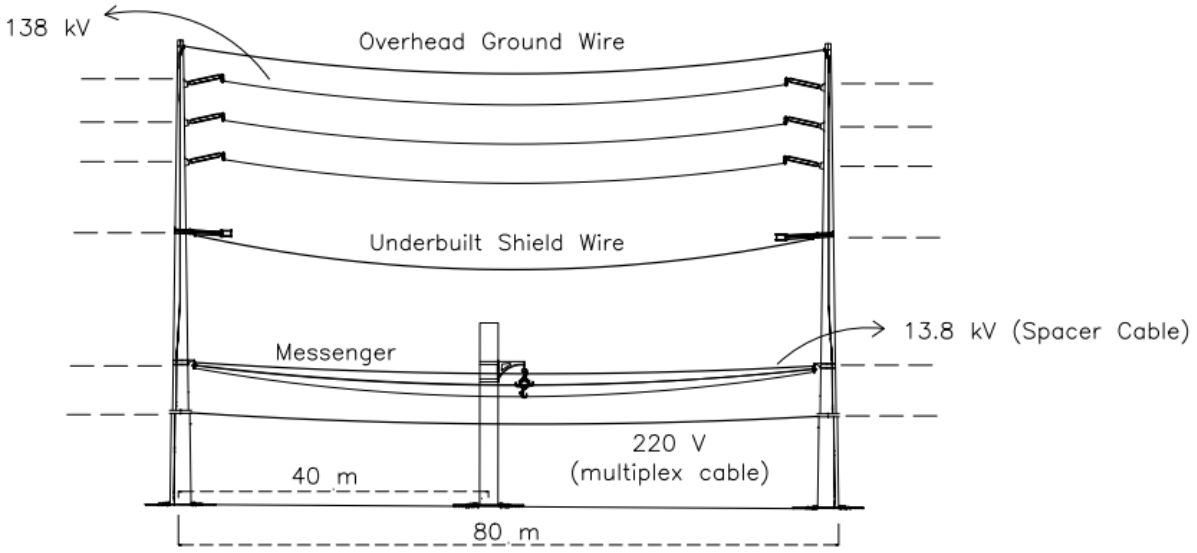

Fig. 2. Hybrid overhead line (BATISTA MORAES et al., 2023).

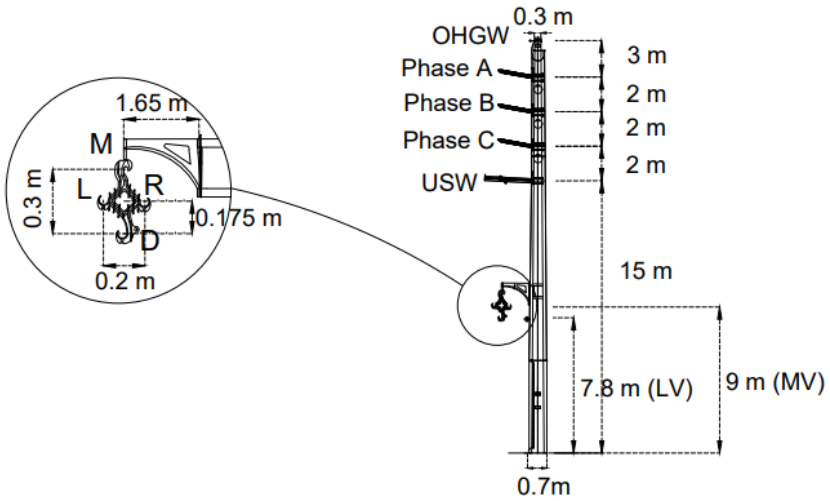

Fig. 3. Detail of the hybrid overhead line (BATISTA MORAES et al., 2023).

2.1 Line

The multi-conductor lines are represented using the wideband model, also known as the Universal Model (MORCHED; GUSTAVSEN; TARTIBI, 1999). This choice was made due to its inherent advantages over the Frequency-Dependent model (MARTI, 1982). Unlike the latter, the wideband model avoids the assumption of a transformation matrix that maintains real and

constant relationships between modal and phase quantities within the frequency range under consideration. Particularly in studies including cable systems, multi-circuit overhead lines, and strongly asymmetric overhead lines, the transformation matrix can exhibit significant frequency dependence (GUSTAVSEN; SEMLYEN, 1998). Addressing this challenge, the Universal Model can be applied to both overhead lines and cables, even with strongly frequency-dependent transformation matrices and markedly distinct modal time delays (MORCHED; GUSTAVSEN; TARTIBI, 1999).

The diameters and d.c. resistances of the line conductors are presented in Table 1.

The influences of the dielectric coatings of the MV and LV conductors were not considered in the simulations. Previous investigations on such influences on the voltages caused by direct (DUGAN; SMITH, 1988) and indirect strokes (LEAL; DE CONTI, 2020) on conventional distribution lines indicate that they can be neglected in practical cases.

Table 1 - Conductors' data.

Conductor	d.c. resistance (Ω/km)	Outer diameter (cm)
OHGW	0.491	1.47
Phase conductor (HV)	0.17	1.83
USW	4.46	0.8
Messenger	3.73	0.95
Phase conductor (MV)	0.253	1.29
Neutral (LV)	0.632	1.35
Phase conductor (LV)	0.3414	1.286

2.2 Grounding

The grounding system is represented by a lumped resistance, the value of which is equal to its impulse impedance (Zg). The impulse impedance is defined as the ratio of maximum values of the ground potential rise and the current at the feeding point. The frequency of soil electrical parameters is not taken into account, which is a conservative approach

Visacro and Silveira (2016) analyzed the response of grounding electrodes subjected to direct stroke currents. For this analysis, computer simulations were carried out using a hybrid electromagnetic model (HEM) for grounding modeling. It is a numerical model based on

electromagnetic field theory that uses circuit concepts and considers all effects of coupling between electrodes. Comparisons were made between the response obtained from typical grounding arrangements using the hybrid model and modeling the ground as an impulse impedance. Different resistivity values and counterpoise cable lengths were considered, and one of the authors' main conclusions is that representing the grounding electrodes by their impulse impedance results in practically the same lightning performance obtained when the study is carried out using the hybrid model. Therefore, modeling grounding as an impulse impedance generates results similar to modeling using a numerical method, with the advantage of being much simpler to implement.

Given the advantages of this approach, in this work the grounding is modeled through its impulse impedance.

2.3 Stroke Current

The stroke current $i(t)$ is represented by the Heidler function (HEIDLER; CVETIĆ, 2002), defined by equations (1) and (2):

$$i(t) = \frac{I_0}{\eta} \frac{(t-\tau_1)^n}{1+(t-\tau_1)^n} \, exp\left(\frac{t}{\tau_2}\right) \tag{1}$$

$$\eta = exp\left[-\left(\frac{\tau_1}{\tau_2}\right)\left(n \, \frac{\tau_2}{\tau_1}\right)^{\frac{1}{n}}\right] \tag{2}$$

The equivalent stroke current front time ($tf_{30\text{-}90}$) is defined as the duration between the points where the wavefront intercepts the 30% and 90% amplitude levels, divided by 0.6 (ANDERSON; ERIKSSON, 1980). The analysis includes stroke current front times ranging from 1 to 8 µs. Table 2 shows the parameters of the Heidler function for each respective front time.

Table 2 - Parameters of the Heidler function (HEIDLER; CVETIĆ, 2002) for the lightning currents considered.

Front Time (µs)	I_0 **(kA)**	τ_1 **(µs)**	τ_2 **(µs)**	**n**	**Wavetail (µs)**
1.0	-29.9	0.31	91.8	2	67.5
2.0	-29.6	0.67	91.8	2	70.1
3.8	-29.3	1.44	91.8	2	74.3
8.0	-29.15	3.65	91.8	2	83.4

2.4 Tower

The tower shown in Fig. 3 is modeled as a constant parameter (CP) lossless transmission line with distributed parameters. The voltages on the tower are calculated assuming different formulas according to different authors for the surge impedance in the case of a lightning hit to the tower top. The calculated voltages were compared to the ones measured on a 1:20 reduced tower model, and then the surge impedance that provides the calculated voltages closest to the measured results was selected for the simulations.

The models in Table 3 provide an average of the impedance over all tower sections; the calculated surge impedance varies from 255 Ω to 336 Ω (variation of 32%). The multistory tower model (ISHII et al., 1991), indicated in Fig. 4, considers different impedances for each tower section. The surge impedances and the parameters of the RL circuits of the different sections were calculated according to (CIGRÉ W.G. C4.23, 2021)and (AMETANI; KAWAMURA, 2005), respectively.

Table 3 - Surge impedances of the tower shown in Fig. 3.

Tower model	Z_s
Chisholm et al. (CHISHOLM; CHOW; SRIVASTAVA, 1985)	255 Ω
Takahashi (TAKAHASHI, 1994)	297 Ω
Wagner and Hileman (WAGNER; HILEMAN, 1960)	336 Ω

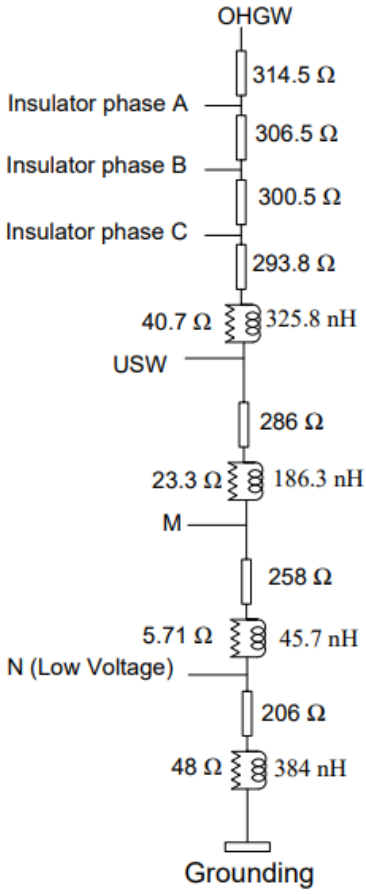

Fig. 4. Multistory tower model (ISHII et al., 1991), with its parameters estimated according to (CIGRÉ W.G. C4.23, 2021) and (AMETANI; KAWAMURA, 2005).

2.4.1 Test Setup

In order to evaluate the results predicted by the different models, a 1:20 scale model of the tower, made of aluminium, was built. It is shown in Fig. 5.

Although the diameters of the top and base of the actual tower are 0.3 m and 0.7 m, respectively, the tower model, 1.2 m high, was cylindrical, with a diameter equal to 2.54 cm, corresponding to 0.5 m. Taking into account the tower height (24 m) and its top and base diameters, the approximation as a cylinder seems reasonable. The ground, simulated by interconnected aluminum plates, can be assumed to be a perfectly conducting plane.

The measured average propagation velocity along the reduced tower model was equal to 0.92 *c*, where *c* is the speed of light in free space. Currents were injected at the top of the tower, and the corresponding voltages were measured according to the test setup shown in Fig. 6(a). The

internal resistance of the pulse generator (PG) is 50 Ω. The function of the 98 Ω resistor is to adjust the current waveform. Fig. 6(b) presents the corresponding circuit in the EMTP.

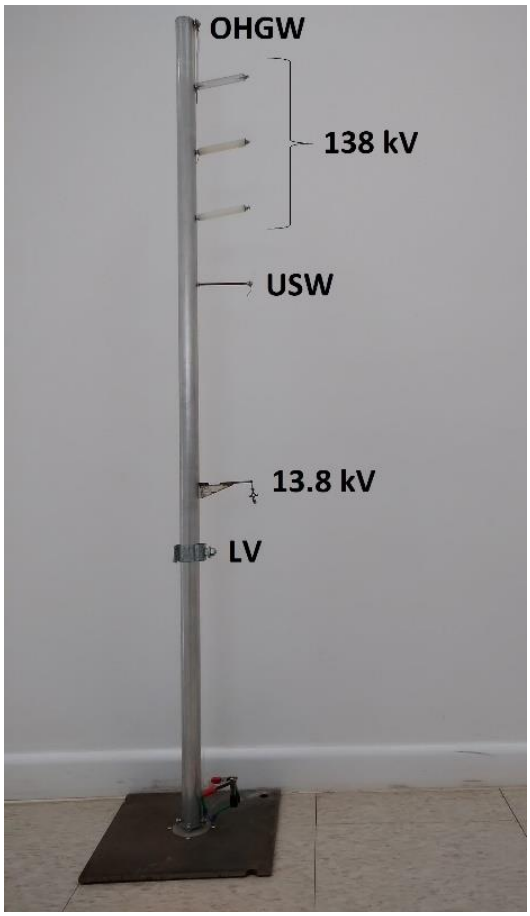

Fig. 5. Reduced scale (1:20) tower model (BATISTA MORAES et al., 2023).

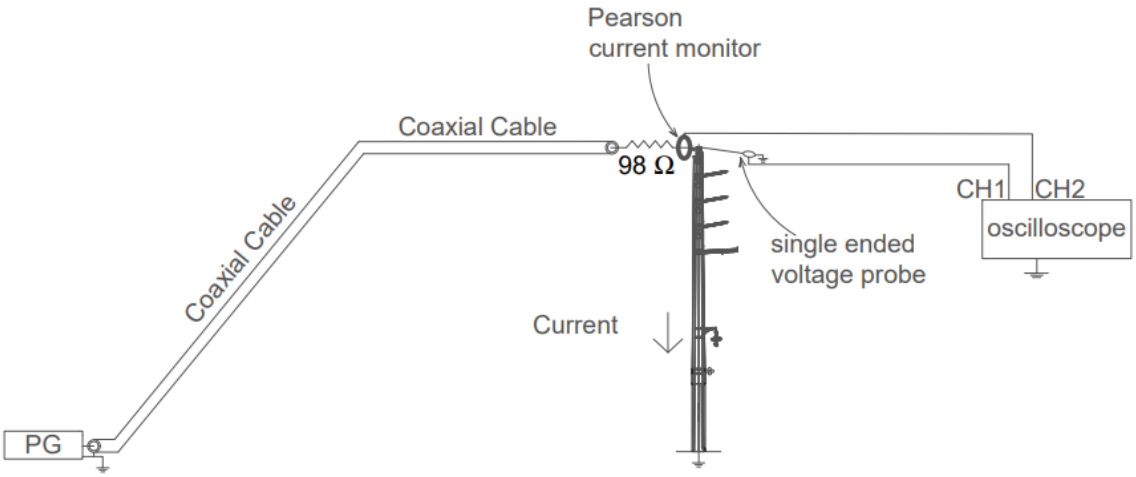

(a)

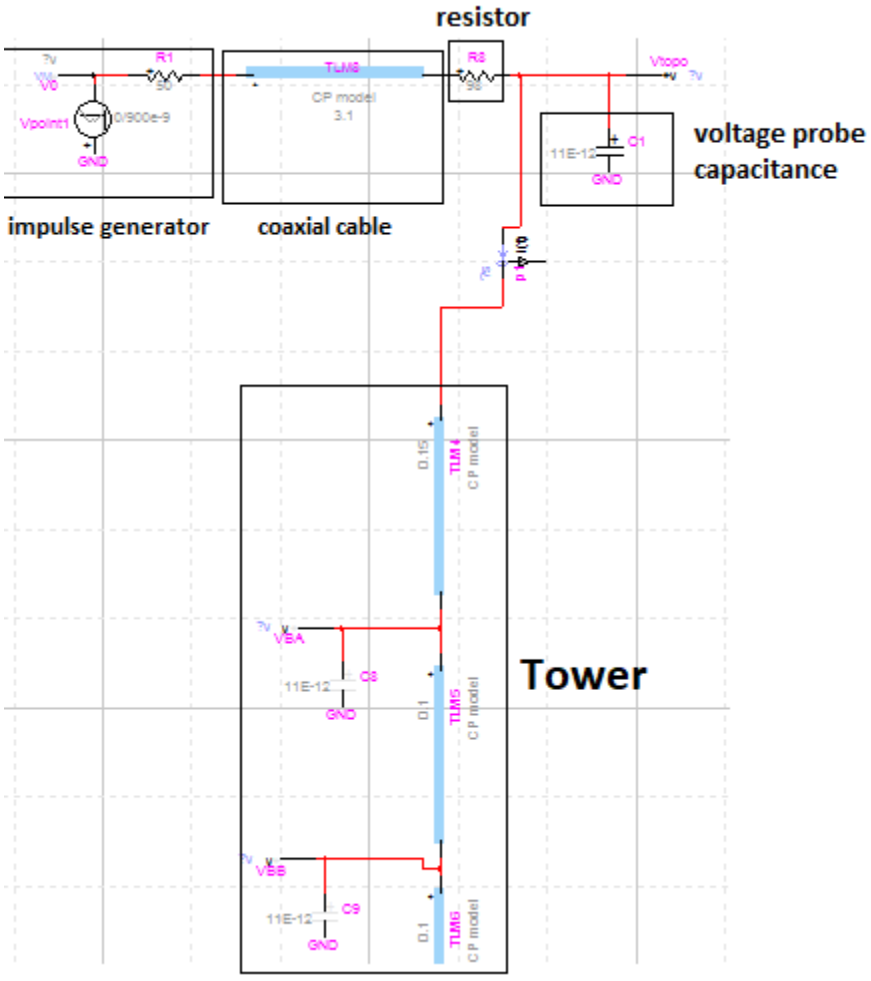

(b)

Fig. 6. Circuits for obtaining measured and calculated voltages at the tower.
a) Sketch of the test setup (adapted from BATISTA MORAES; PIANTINI; SHIGIHARA, 2023b)
b) EMTP modeling of the circuit showed in Fig 6(a).

In the experiments, the current was injected into the tower through a horizontal coaxial cable (3.1 m long) and measured by a Pearson current monitor model 2877. The measuring system bandwidth was from d.c. to 200 MHz. High-impedance probes with a capacitance of 11 pF and bandwidth from d.c. to 500 MHz were used for measuring the voltages. The sampling rate and bandwidth of the oscilloscope (Agilent, model DSO-X 3032A) were 2 GSamples/s and 350 MHz, respectively. The input voltage source was generated by a waveform generator Agilent 33521A 250 MSamples/s and 30 MHz (BATISTA MORAES et al., 2022).

Baba and Ishii (1997) showed that the measurements are affected by the arrangement of the current conductor and the voltage measurement wire. They concluded that a vertical current lead wire results in a surge impedance value about 20% higher than that measured with a horizontal current lead wire. In the tests performed in this study, the measurements were performed with a horizontal current lead wire.

2.4.2 Comparisons between measured and calculated voltages on the tower

Considering the test circuit shown in Fig. 6, a comparison between the measured current with the ones calculated assuming the values of the tower surge impedance indicated in Table 3 (Chisholm et al. (CHISHOLM; CHOW; SRIVASTAVA, 1985), Takahashi (TAKAHASHI, 1994), Wagner and Hileman (WAGNER; HILEMAN, 1960)) and in Fig. 4 (multistory model (ISHII et al., 1991)) is presented in Fig. 7. The calculations were performed using the EMTP (PGSTECH; POWERSYS, 2023). The agreement with the measured current can be considered reasonable for all the models used for calculating the tower surge impedance.

The measured and calculated voltages at the tower top are compared in Fig. 8. All the models lead to similar results, but the tower impedances that lead to voltage peak values closer to the measured one were those calculated using the Takahashi (TAKAHASHI, 1994) and Chisholm et al. (CHISHOLM; CHOW; SRIVASTAVA, 1985) models. The deviations of the calculated voltage peaks in relation to the measured one are presented in Table 4. Comments on the observed differences will be presented later in this subsection (before Table 5).

Additional tests were then performed, with six measurements along the tower. The voltage probe was placed at the points indicated in Fig. 9.

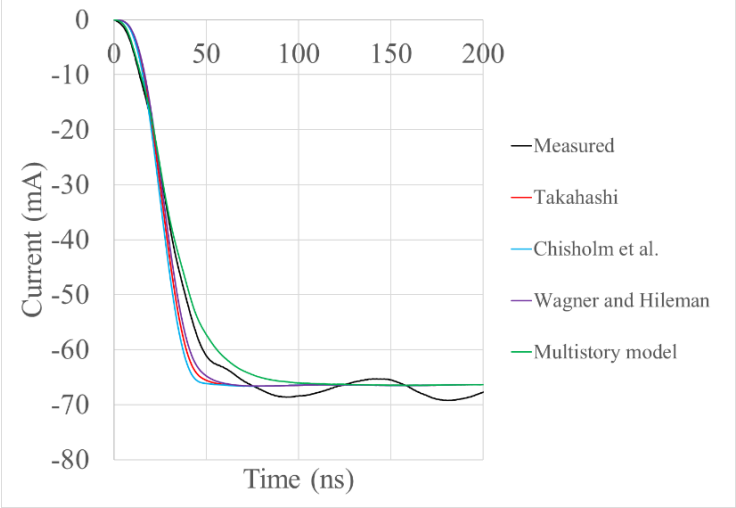

Fig. 7. Measured and calculated currents injected at the tower top (BATISTA MORAES; PIANTINI; SHIGIHARA, 2023b).

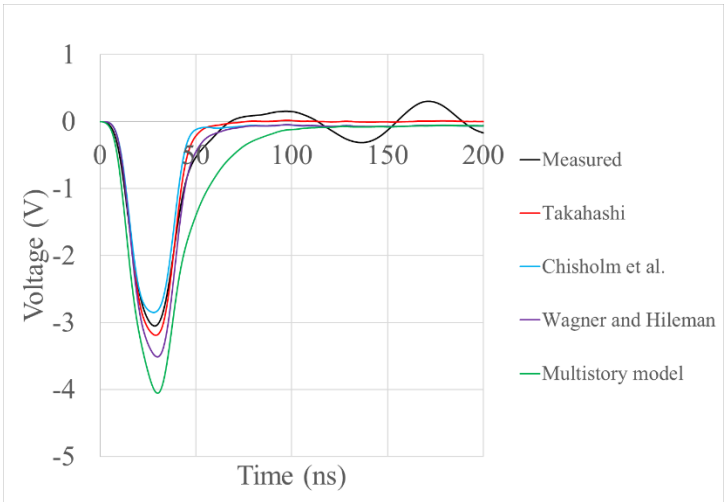

Fig. 8. Measured and calculated voltages at the tower top (BATISTA MORAES; PIANTINI; SHIGIHARA, 2023b)

Table 4 - Deviations of the calculated voltage peaks (Fig. 8) at the tower top in relation to the measured one.

Tower model	$\left(\frac{\mathbf{V_{calculated}} - \mathbf{V_{measured}}}{\mathbf{V_{measured}}}\right) * \mathbf{100\%}$
Chisholm et al. (CHISHOLM; CHOW; SRIVASTAVA, 1985)	-6.6%
Multistory (ISHII et al., 1991)	32.9%
Takahashi (TAKAHASHI, 1994)	4.5%
Wagner and Hileman (WAGNER; HILEMAN, 1960)	15.1%

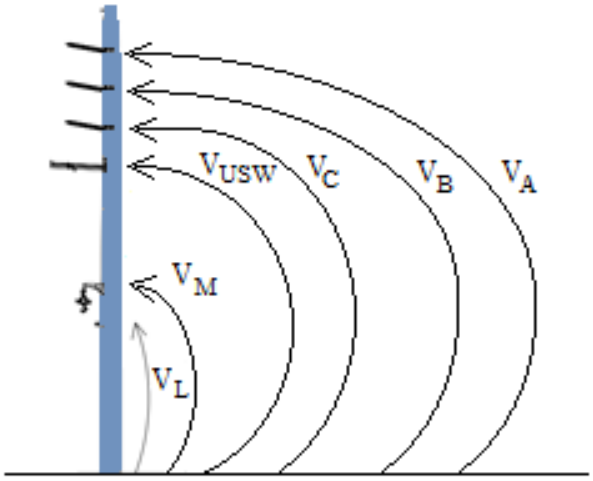

Fig. 9. Measured voltages between the top of the tower and the ground (BATISTA MORAES; PIANTINI; SHIGIHARA, 2023b).

In Fig. 9, V_A, V_B, and V_C are the voltages between the bases of the insulators of the phases A, B, and C, respectively, and the ground. V_{USW}, V_M, and V_L are the voltages between the underbuilt shield wire and ground, between the messenger of the MV line and ground, and between the neutral of the LV line and ground, respectively. Actually, there were no line conductors during the tests; hence V_{USW} represents the voltage between the point where the underbuilt shield wire is placed and the ground. The same observation holds for V_M and V_L.

Comparisons between measured and calculated voltages, considering the Takahashi model (TAKAHASHI, 1994) and the six positions indicated in Fig. 9, are presented in Figs. 10 to 15.

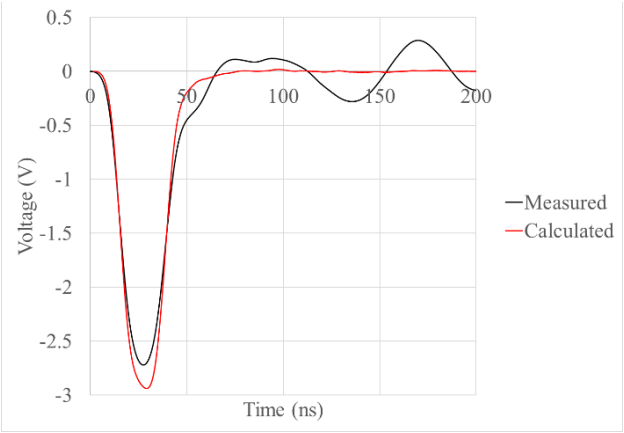

Fig. 10. Measured and calculated voltages (Takahashi model (TAKAHASHI, 1994)) between the base of insulator A and ground (VA, Fig. 9) (BATISTA MORAES; PIANTINI; SHIGIHARA, 2023b).

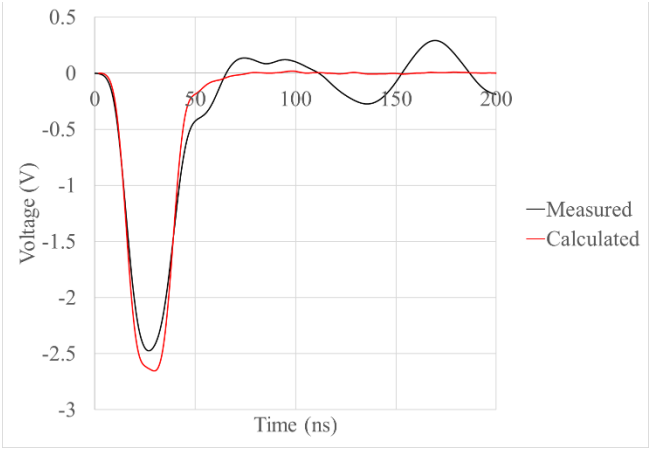

Fig. 11. Measured and calculated voltages (Takahashi model (TAKAHASHI, 1994)) between the base of insulator B and ground (VB, Fig. 9) (BATISTA MORAES; PIANTINI; SHIGIHARA, 2023b).

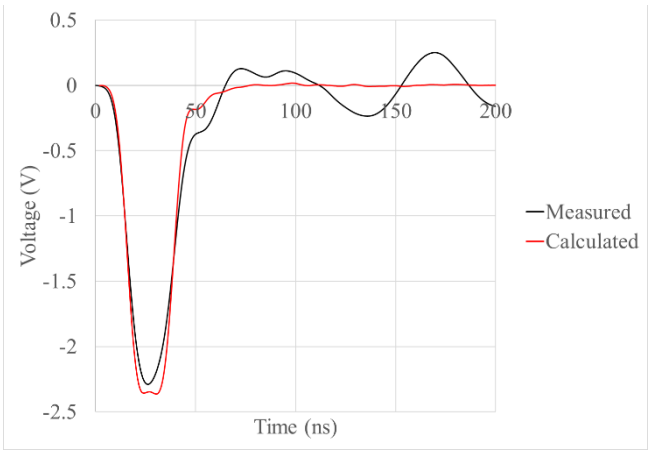

Fig. 12. Measured and calculated voltages (Takahashi model (TAKAHASHI, 1994)) between the base of insulator C and ground (VC, Fig. 9) (BATISTA MORAES; PIANTINI; SHIGIHARA, 2023b).

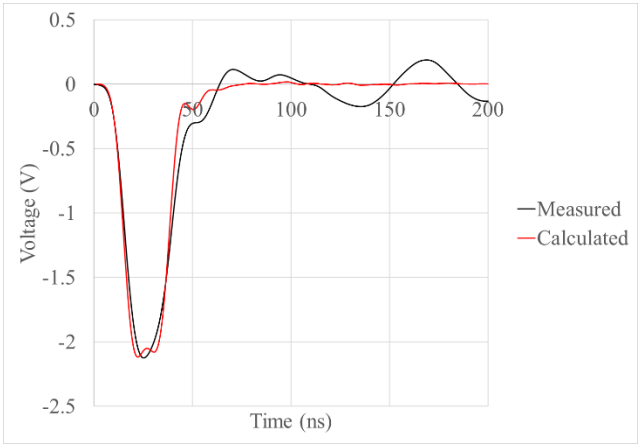

Fig. 13. Measured and calculated voltages (Takahashi model (TAKAHASHI, 1994)) between the point where the underbuilt shield wire is connected and ground (VUSW, Fig. 9) (BATISTA MORAES; PIANTINI; SHIGIHARA, 2023b).

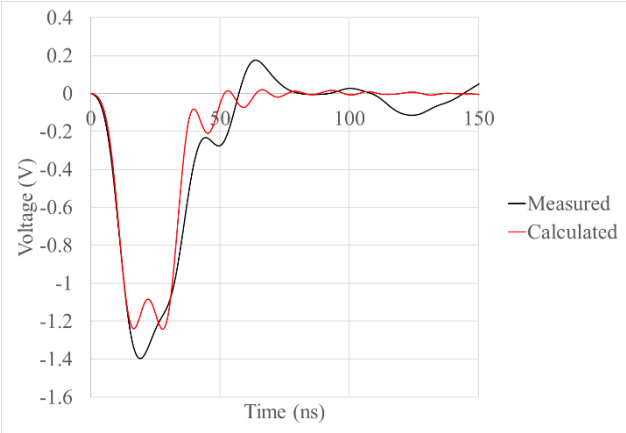

Fig. 14. Measured and calculated voltages (Takahashi model (TAKAHASHI, 1994)) between the point where the messenger is connected and ground (VM, Fig. 9) (BATISTA MORAES; PIANTINI; SHIGIHARA, 2023b).

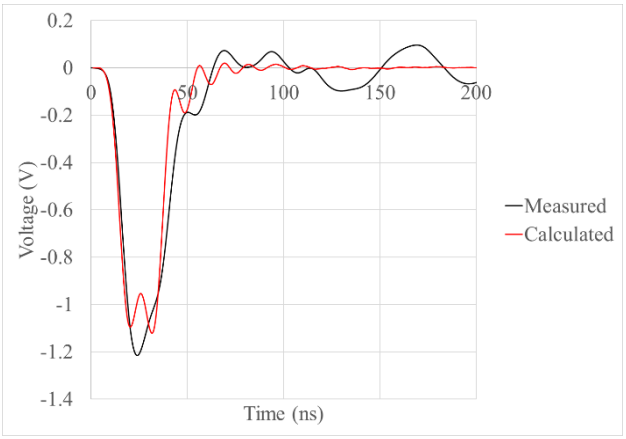

Fig. 15. Measured and calculated voltages (Takahashi model (TAKAHASHI, 1994)) between the point where the neutral of the LV line is connected and ground (VL, Fig. 9) (BATISTA MORAES; PIANTINI; SHIGIHARA, 2023b).

Figs. 10 to 15 show that the tower surge impedance calculated according to the Takahashi's model (TAKAHASHI, 1994) leads to voltages very similar to the measured ones in magnitude and waveform at all the observed points along the tower.

The deviations of the calculated peak voltages in relation to the measured ones, at the seven points along the tower, are presented in Table 5. The deviations are calculated according to (3):

$$Deviation = \left(\frac{V_{calculated} - V_{measured}}{V_{measured}}\right) 100\% \quad (3).$$

Large differences are observed between the mean absolute values of the deviations, as well as between the maximum deviations. The mean absolute values varied from 5.8% (Wagner and Hileman (WAGNER; HILEMAN, 1960)) to 29.4% (Multistory model (ISHII et al., 1991), with

the parameters estimated according to (CIGRÉ W.G. C4.23, 2021) and (AMETANI; KAWAMURA, 2005)). Regarding the maximum deviations, the range was from 11.1% (Takahashi (TAKAHASHI, 1994)) to 45.9% (Multistory model). The point along the tower corresponding to the maximum deviation of the calculated voltage varies with the method adopted for calculating the tower impedance, as can be seen in Table 5. For the Takahashi model, the maximum deviation corresponds to the voltage between the point where the messenger of the MV line is placed and the ground (V_M, Fig. 9).

The suitability of Takahashi's model has also been verified by (MARQUES COSTA et al., 2020) for the case of lattice towers with heights varying from 50 m to 300 m by comparing the calculated surge impedances with those obtained using the Finite Element Method.

In conclusion, all the models reproduced the characteristics of the measured voltages along the tower reasonably well, but for the specific tower considered in this study, the surge impedances estimated using the methods by Takahashi and by Wagner and Hileman led to the slightest deviations between measured and calculated peak voltages along the tower. Based on the obtained results, the Takahashi's model, shown in Fig 16, was chosen to represent the tower.

Table 5 - Deviations of the calculated voltages in relation to the measured ones (%).

Voltage	Takahashi	Wagner and Hileman	Chisholm et al.	Multistory
V tower top	4.5	15.1	-6.6	32.9
V_A	8.0	12.6	-9.2	37.7
V_B	7.2	3.9	-9.7	43.1
V_C	3.2	6.8	-11.8	45.9
V_{USW}	-0.3	1.1	-15.2	18.8
V_M	-11.1	0.9	-18.7	14.8
V_L	-7.8	-0.4	-20.7	12.7
Mean absolute value of deviations	**6.0**	**5.8**	**13.1**	**29.4**
Maximum deviation (absolute value)	**11.1**	**15.1**	**20.7**	**45.9**

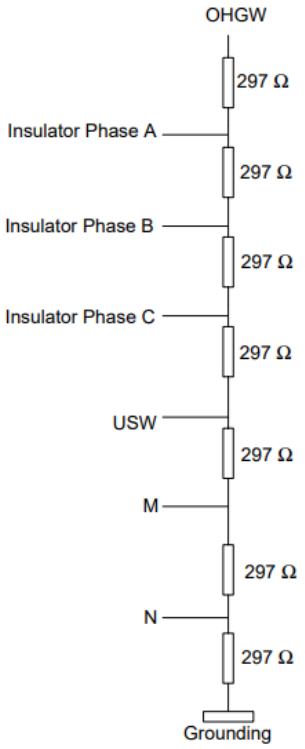

Fig. 16. Tower model according to the Takahashi's method (BATISTA MORAES et al., 2023).

2.5 Insulators

The high voltage insulators are represented as 75 pF capacitors. This value was obtained through measurements on a 138 kV polymeric insulator, conducted at a frequency of 428.7 kHz, in an arrangement resembling an actual line setup. The equipment used to measure the insulator capacitance has an inductance whose value is known. After connecting the insulator, a sinusoidal current flows through the LC circuit and the resonance frequency is measured. The obtained value was 428.7 kHz. Once the frequency and inductance values are known, the capacitance value is calculated. The evaluation of flashover events is carried out using the Integration Method (WITZKE; BLISS, 1950, DARVENIZA, 1988, CALDWELL; DARVENIZA, 1973, CHOWDHURI; MISHRA; MCCONNELL, 1997, ANCAJIMA et al., 2007), represented by (4):

$$DE = \int_{t_0}^{t_c} [V(t) - V_0]^k dt \tag{4}$$

where t_0 is the time when the applied voltage V(t) surpasses V_0, which is the minimum voltage to start the breakdown process, and t_c is the time-to-breakdown. Breakdown occurs if DE exceeds a critical threshold (DE_C).

The volt-time (V-t) curves corresponding to four lightning impulses, representative of the potential overvoltages across the HV line insulators in the event of direct strikes on a tower, were obtained in (BATISTA MORAES; PIANTINI; SHIGIHARA, 2023a). The applied impulses had the following waveforms: 1.2/6 µs, 1.2/50 µs, 2/10 µs, and 2.5/14 µs. Using the V-t curves for each impulse, the insulator responses to these overvoltages were modeled by obtaining the parameters V_0, k, and DE_C that allow to reproduce the observed insulator behaviors.

2.5.1 Test Setup

The insulator test setup, depicted in Fig. 17 and Fig. 18, aimed at simulating conditions similar to those the insulator would be submitted to when installed in a real line.

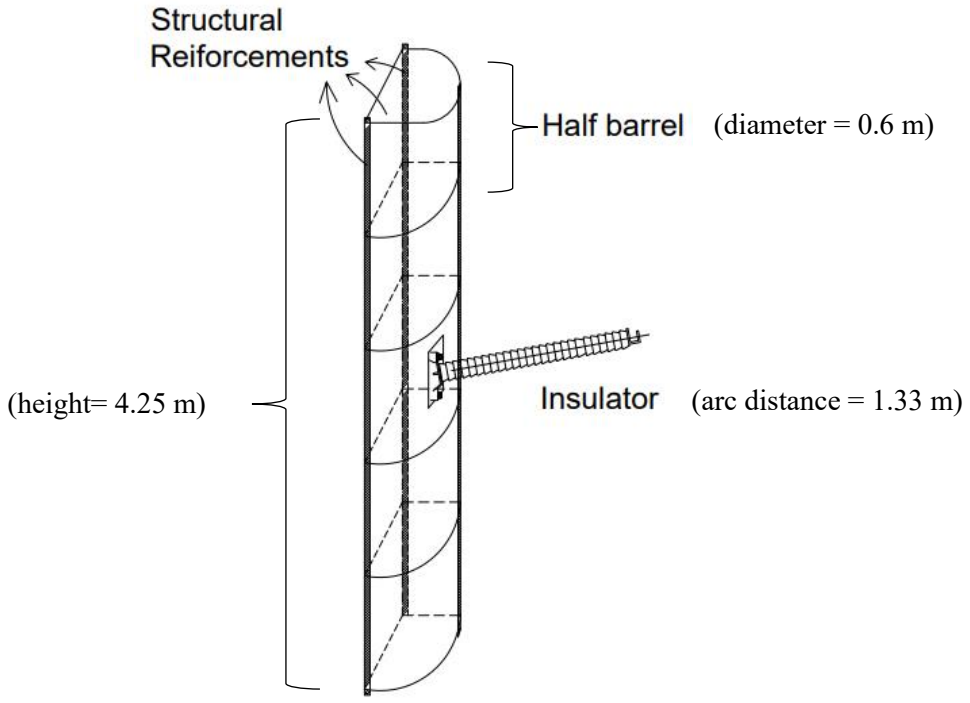

Fig. 17. Sketch of the insulator test setup (adapted from BATISTA MORAES; PIANTINI; SHIGIHARA, 2023a).

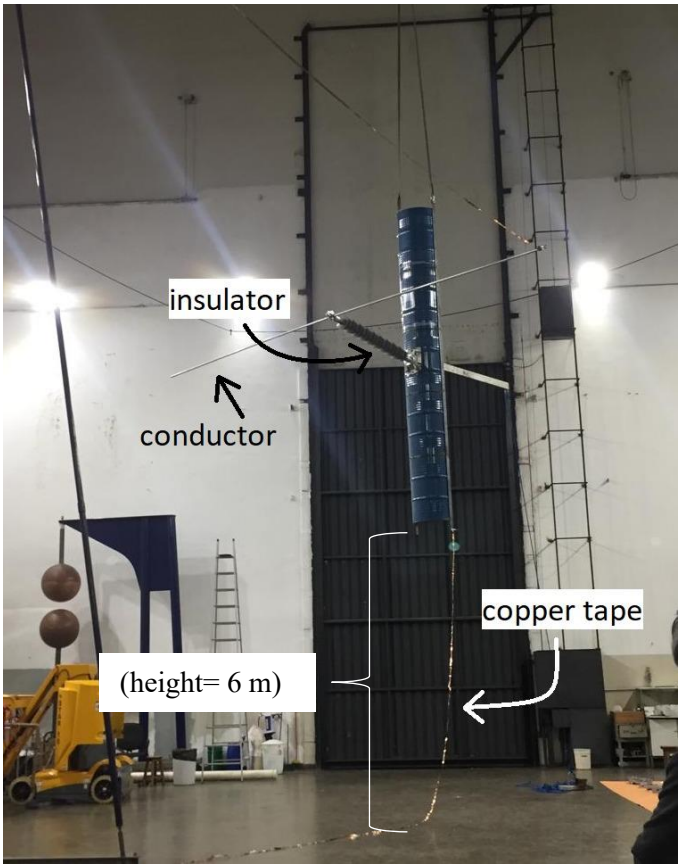

(a)

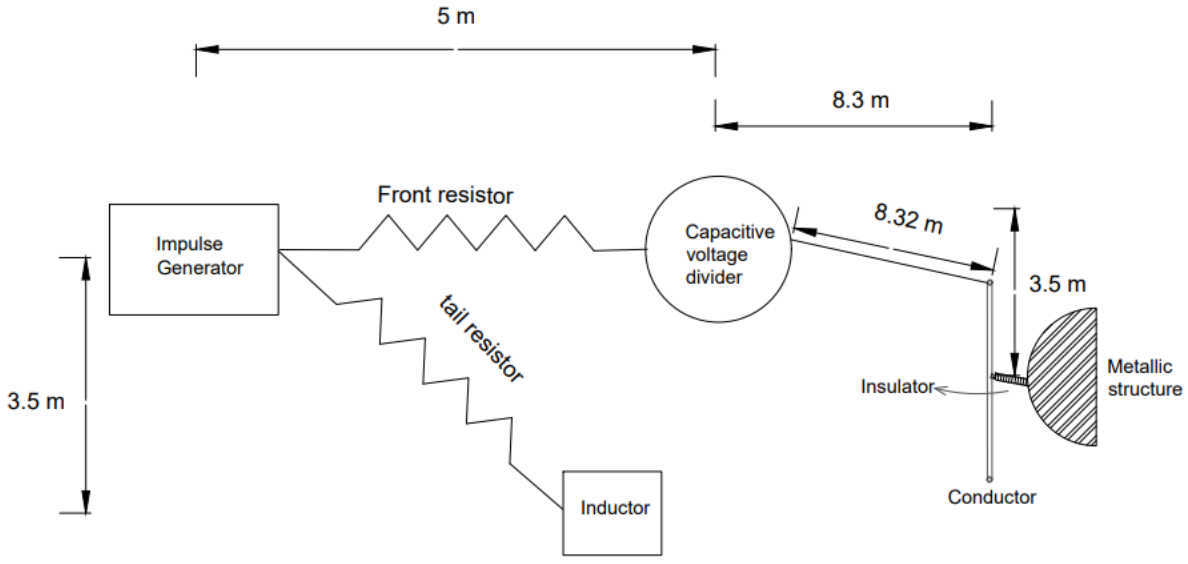

(b)

Fig. 18. High voltage tests performed in laboratory.
a) Picture of the assembled setup (adapted from BATISTA MORAES; PIANTINI; SHIGIHARA, 2023a).
b) Top view of the insulator test setup (not to scale).

The metallic structure was made with metal barrels that were split in half and then welded together. Then, the metallic structure was placed 6 m above the ground, as shown in Fig. 18(a), to avoid the influence of the stray capacitances that connect the structure and the ground. A copper tape was used to connect the structure and the ground..

The high-voltage laboratory tests were conducted at the High Voltage Laboratory of the Institute of Energy and Environment of the University of São Paulo (IEE-USP) using a Marx impulse generator with 15 stages and a maximum voltage of 3 MV, total energy of 225 kJ, and total capacitance of 50 nF. The tests were performed according to the procedure specified in (IEC 60060-1, 2010) with parameters that varied according to the impulse waveshape. Examples of configurations suitable for generating typical non-standard lightning impulse voltages can be found in (SHIGIHARA et al., 2018). The test circuit also contains a capacitive voltage divider (3 MV, three stages, 1440 pF/stage, ratio (three stages): 2700:1)

The representative voltage waveshapes were chosen based on simulations carried out using EMTP (PGSTECH; POWERSYS, 2023) with the objective of verifying the characteristics of the overvoltages that the insulators would be exposed to in the case of a direct lightning strike to a line tower.

The line considered in the simulations to obtain the waveshapes has 22 spans (see Fig 2), and the simulations were run for the case of a direct strike to the top of the central tower. The current was represented by an ideal source and a Heidler function (HEIDLER; CVETIĆ, 2002). The magnitude was 31 kA, the time to half-value was 70 μs, and its front time varied from 1 μs to 10 μs. The grounding system was represented by its impulse impedance, which varied in the range of 10 Ω to 1000 Ω. The soil resistivity was equal to 1000 Ωm. The conductors' heights were considered constant and equal to the heights at the tower (showed in Fig. 3). The tower surge impedance was equal to 297 Ω (as shown in subsection 2.4). For each case, the overvoltage across the insulator terminals of phase A of the 138 kV line (the highest insulator, as shown in Fig. 3) was calculated.

The voltages obtained from the simulations were grouped according to their similarity. An example of a group of voltages with similar characteristics is shown in Fig. 19. The peak values are normalized, as the focus was on the waveshapes. The voltages correspond to the following combinations of the values of the impulse impedance (Zg) and stroke current front time (t_f): Zg = 200 Ω, t_f = 5 μs; Zg = 100 Ω, t_f = 5 μs; and Zg = 20 Ω, t_f = 6 μs. In the laboratory tests,

this group of voltages was represented by the 1.2/6 µs impulse, which, as shown in Fig. 20, is relatively similar to the calculated voltages.

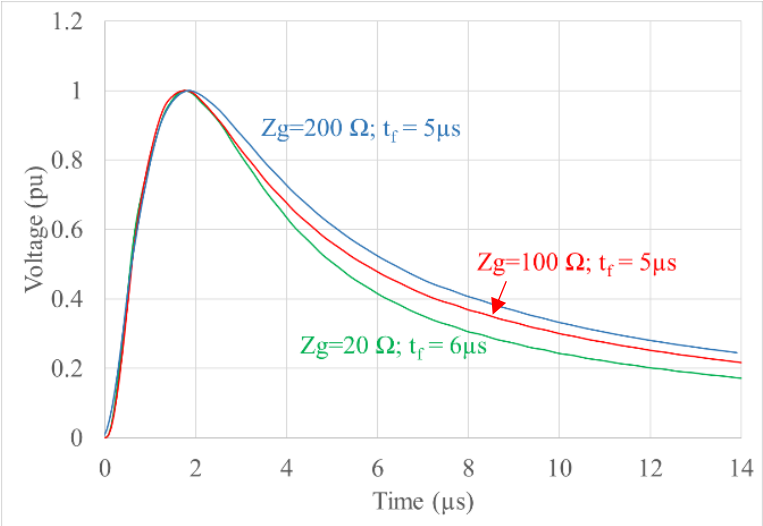

Fig. 19. Example of a group of calculated voltages with relatively similar characteristics (BATISTA MORAES; PIANTINI; SHIGIHARA, 2023a).

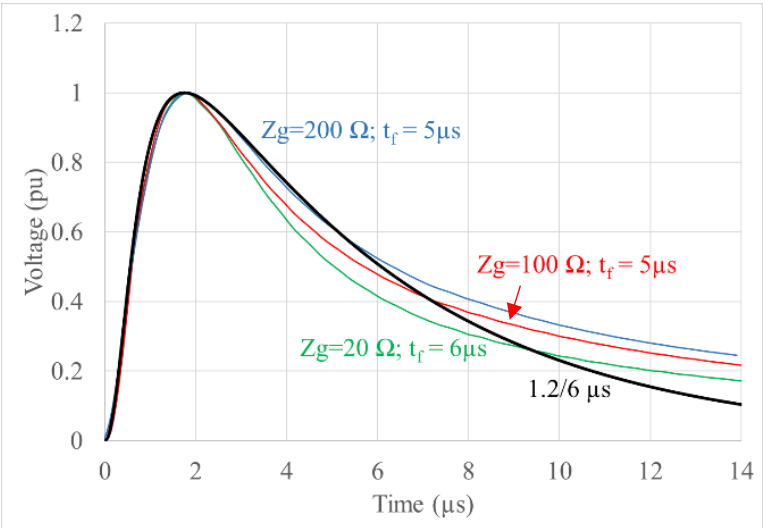

Fig. 20. Comparison of the calculated voltages shown in Fig. 19 and the 1.2/6 µs impulse waveshape (BATISTA MORAES; PIANTINI; SHIGIHARA, 2023a).

The other two non-standard waveshapes, namely 2/10 µs and 2.5/14 µs, were chosen following the same procedure, i.e., by selecting two other groups of voltage impulses whose waveshapes could be reproduced at the High Voltage Laboratory. The standard impulse (1.2/50 µs) was also included because for very high values of the impulse impedance and long stroke current front

times, the voltage times to half-value may reach a few tens of microseconds. For example, for Zg =1000 Ω and t_f = 10 μs, the time to half-value of the voltage is about 35 μs.

With the CFO values and V-t curves obtained from the tests, additional EMTP simulations were run to obtain the values of the parameters V_0, k, and DE_C so that the insulator model's response could reasonably well reproduce the V-t curves corresponding to the four impulse waveshapes considered.

The Integration Method parameters for the MV voltage spacer were obtained using laboratory test data considering a 15 kV class spacer and bare cables. To consider the influence of the XLPE coverage of the spacer network, the value of 100 kV was added at each point of the V-t curve, shifting it 100 kV upwards, following the procedure adopted by (BORGHETTI et al., 2018b).

The parameters proposed for the HV insulators and MV spacers for positive and negative polarities are presented in Table 6 and Table 7, respectively. These parameters were obtained by the trial and error method, taking those proposed by Hileman as initial values.

For comparison purposes, the Integration Method parameters were also calculated according to the procedure by (HILEMAN, 1999), using (5) and (6). The corresponding parameter values are indicated in Table 8 and Table 9 considering positive and negative polarities, respectively.

$$V_0 = 0.77\ CFO \tag{5}$$

$$DE_C = 1.1506\ CFO^{\,k} \quad \text{(CFO in volts)} \tag{6}$$

Table 6 - Parameters of the Integration Method for the HV insulators and MV spacers, positive polarity.

Equipment	**Integration Method parameters**		
	V_0 (kV)	k	DE_C (1 μs base)
Insulator (138 kV)	580	1.35	143
Spacer (13.8 kV)	189.4	1.36	31

Table 7 - Parameters of the Integration Method for the HV insulators and MV spacers, negative polarity.

Equipment	Integration Method parameters		
	V_0 (kV)	k	DE_C (1 μs base)
Insulator (138 kV)	645	1.35	92
Spacer (13.8 kV)	240	1.36	12

Table 8 - Parameters of the Integration method for the HV insulators and MV spacers, positive polarity, according to Hileman (HILEMAN, 1999).

Equipment	Integration Method parameters (Hileman).		
	V_0 (kV)	k	DE_C (1μs base)
Insulator (138 kV)	606	1.36	120
Spacer (13.8 kV)	189.4	1.36	24.7

Table 9 - Parameters of the Integration method for the HV insulators and MV spacers, negative polarity, according to Hileman (HILEMAN, 1999).

Equipment	Integration Method parameters (Hileman).		
	V_0 (kV)	k	DE_C (1μs base)
Insulator (138 kV)	763	1.36	164
Spacer (13.8 kV)	210	1.36	28.45

2.5.2 Model validation

Figs. 21 to 30 show the measured and calculated points of the V-t curves of the voltage impulses considered for positive and negative polarities. The tests at the HV Laboratory were performed in different days, with the ambient conditions varying in the following range:

- temperature: 19,07ºC to 21.9ºC;
- humidity: 60% to 72.12%;
- pressure: 93.43 kPa to 94.31 kPa.

The voltages are referred to the standard conditions of temperature, humidity, and pressure according to (IEC 60060-1, 2010). The respective tendency lines, also presented in the figures, were obtained by fitting a power regression.

Figs. 21 and 22 show the measured and calculated V-t curves of the 138 kV insulator for the 1.2/6 µs impulse for positive and negative polarities, respectively.

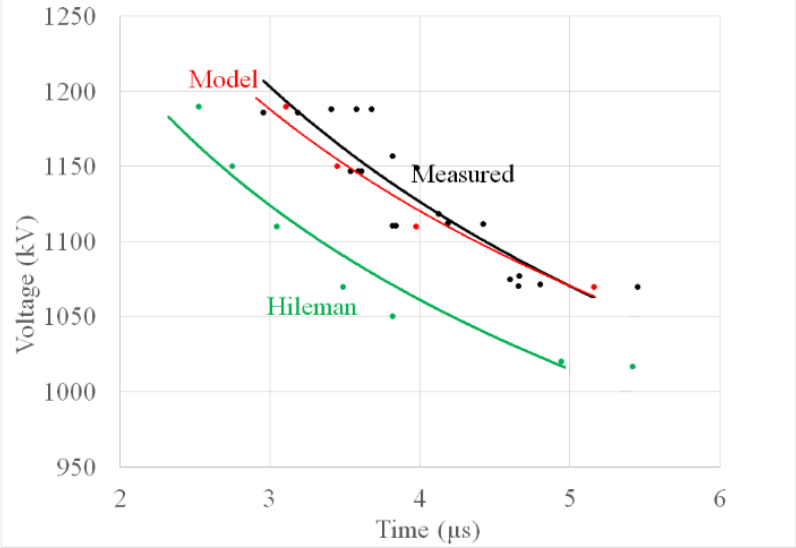

Fig. 21. Measured and calculated V-t curves of the 138 kV insulators for the 1.2/6 µs impulse, positive polarity (BATISTA MORAES; PIANTINI; SHIGIHARA, 2023a).

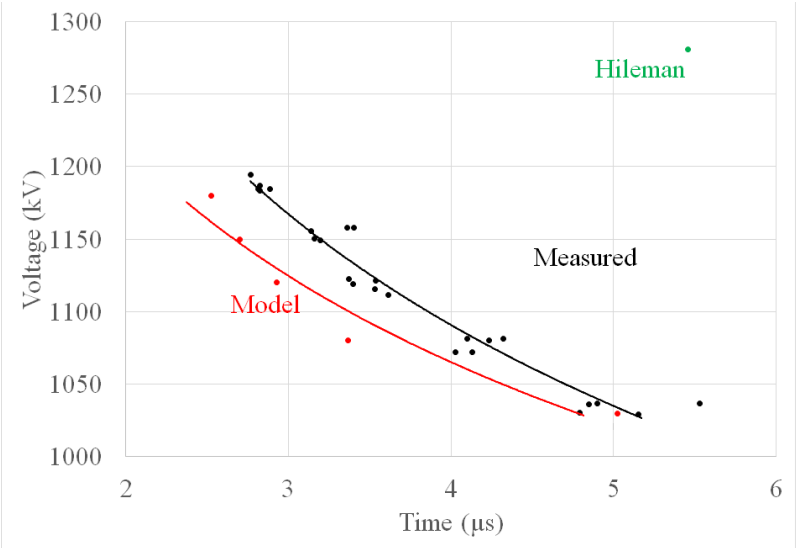

Fig. 22. Measured and calculated V-t curves of the 138 kV insulators for the 1.2/6 µs impulse, negative polarity (BATISTA MORAES; PIANTINI; SHIGIHARA, 2023a).

Figs. 23 and 24 show the measured and calculated V-t curves of the 138 kV insulator for the 2/10 µs impulse for positive and negative polarities, respectively.

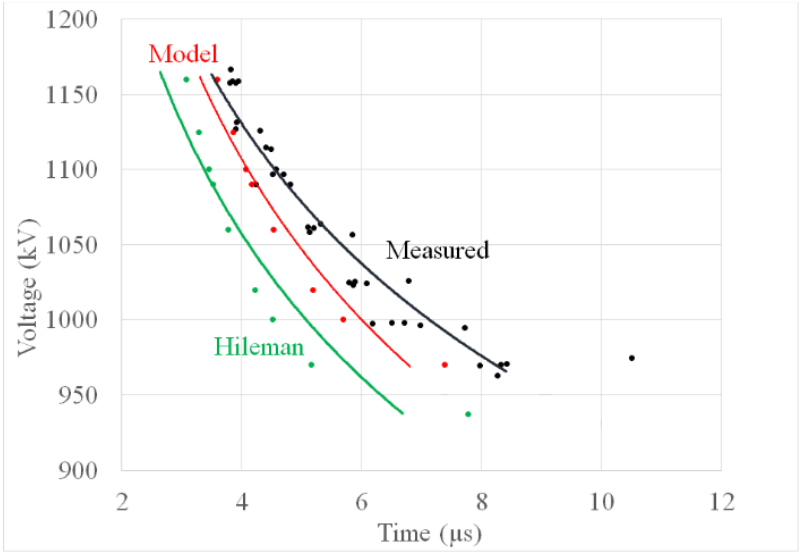

Fig. 23. Measured and calculated V-t curves of the 138 kV insulators for the 2/10 µs impulse, positive polarity (BATISTA MORAES; PIANTINI; SHIGIHARA, 2023a).

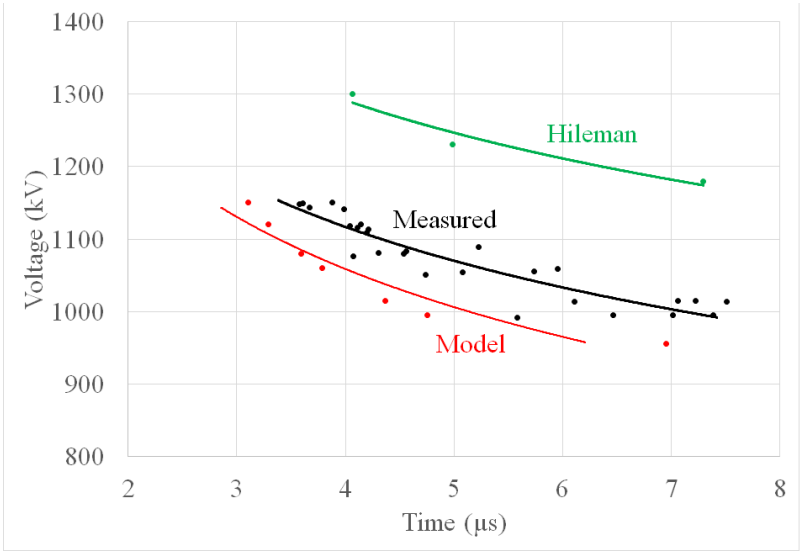

Fig. 24. Measured and calculated V-t curves of the 138 kV insulators for the 2/10 µs impulse, negative polarity (BATISTA MORAES; PIANTINI; SHIGIHARA, 2023a).

Figs. 25 and 26 show the measured and calculated V-t curves of the 138 kV insulator for the 2.5/14 µs impulse for positive and negative polarity, respectively.

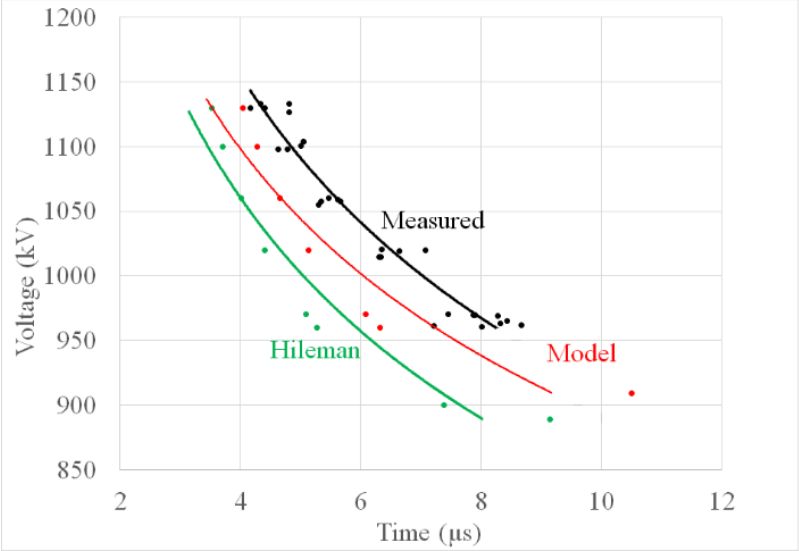

Fig. 25. Measured and calculated V-t curves of the 138 kV insulators for the 2.5/14 μs impulse, positive polarity.

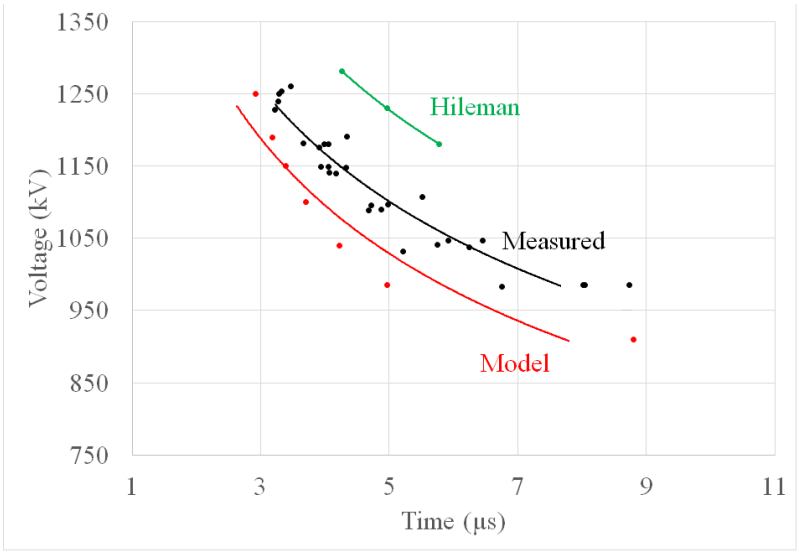

Fig. 26. Measured and calculated V-t curves of the 138 kV insulators for the 2.5/14 μs impulse, negative polarity.

Figs. 27 and 28 show the measured and calculated V-t curves of the 138 kV insulator for the 1.2/50 μs impulse for positive and negative polarities, respectively.

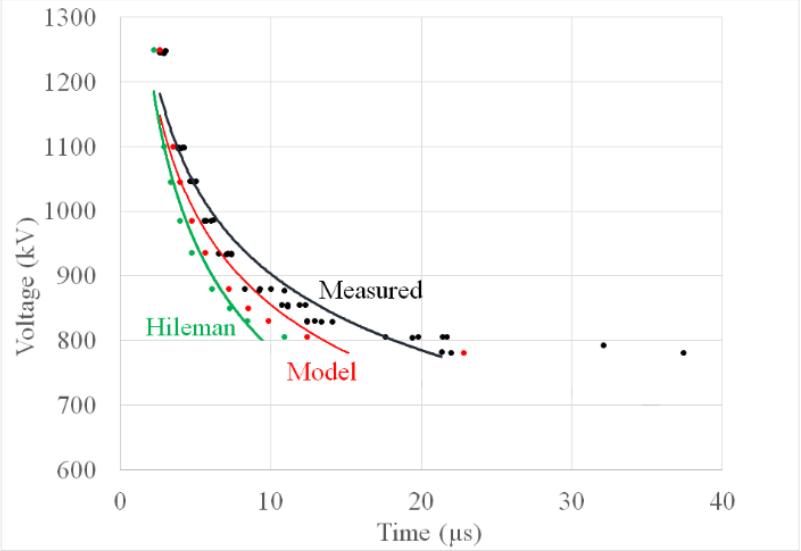

Fig. 27. Measured and calculated V-t curves of the 138 kV insulators for the 1.2/50 µs impulse, positive polarity.

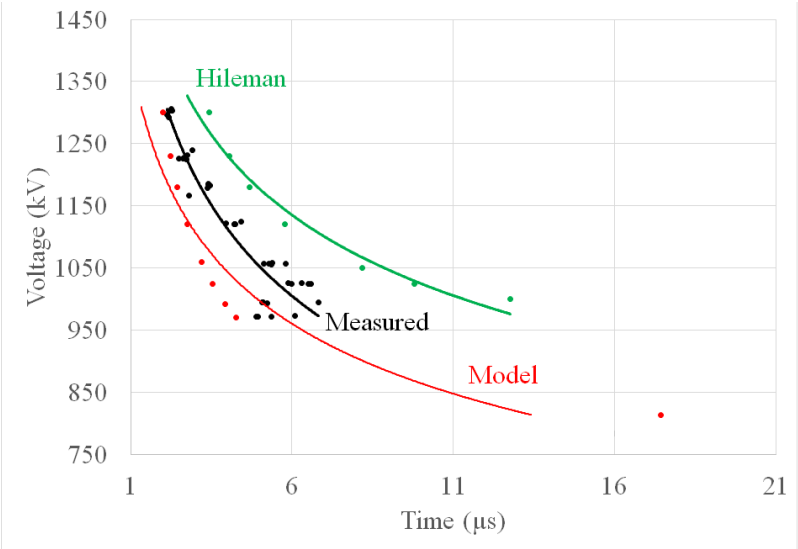

Fig. 28. Measured and calculated V-t curves of the 138 kV insulators for the 1.2/50 µs impulse, negative polarity.

The measured and calculated V-t curves of the MV line spacer (1.2/50 µs waveshape), considering the effect of the XLPE coating, are presented in Figs. 29 and 30 considering positive and negative polarities, respectively.

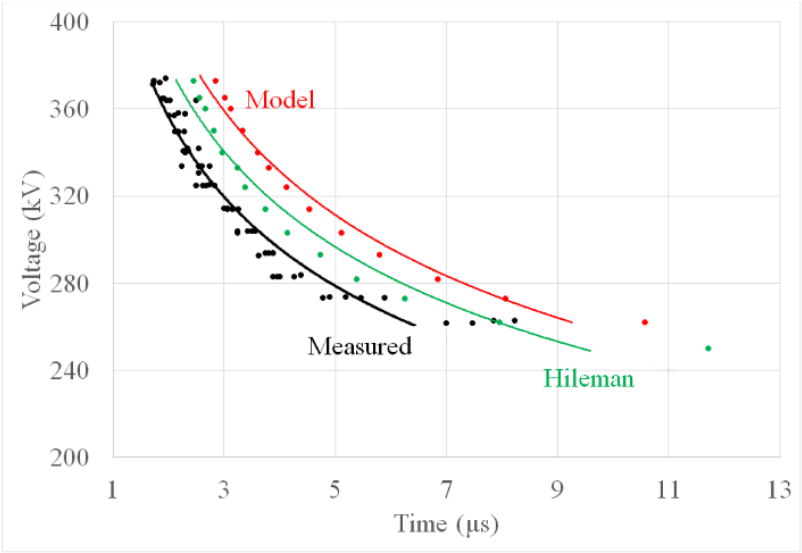

Fig. 29. Measured and calculated V-t curves of the MV line spacer for the 1.2/50 µs impulse, positive polarity (BATISTA MORAES; PIANTINI; SHIGIHARA, 2023a).

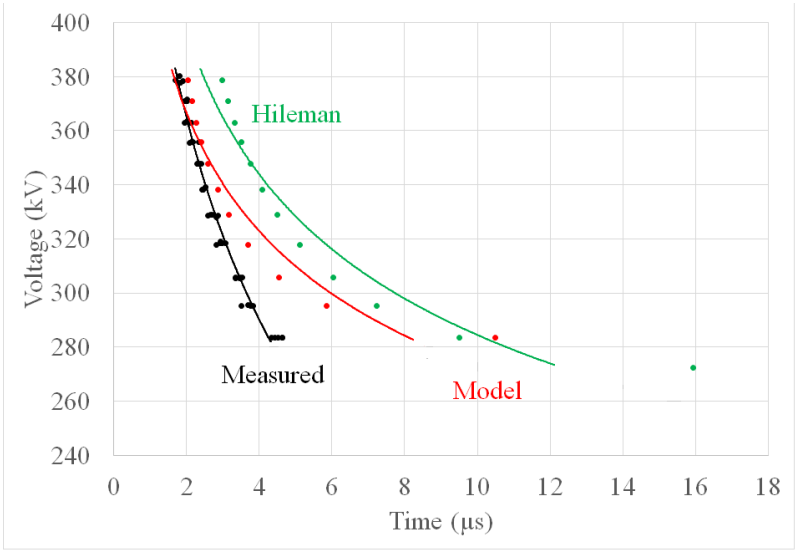

Fig. 30. Measured and calculated V-t curves of the MV line spacer for the 1.2/50 µs impulse, negative polarity (BATISTA MORAES; PIANTINI; SHIGIHARA, 2023a).

For the four impulse voltage impulses of both polarities considered in this investigation, the 138 kV insulator model predicted the occurrence of flashovers for all the voltage values corresponding to the measured V-t curves. The maximum differences between measured and calculated times to breakdown were 7.6 µs for the positive polarity (1.2/50 µs waveshape) and 2.85 µs for the negative polarity (2.5/14 µs waveshape). The mean differences between measured and calculated times to breakdown were 1.16 µs and 1.12 µs for the positive and negative polarities, respectively. These differences are due to factors such as the natural

dispersion of the test results and the imprecision in the parameters' values necessary for the application of the Integration Method.

However, in some cases the model predicted flashovers that did not occur in the tests. For the 2.5/14 μs impulse of positive polarity, the model predicts flashover for voltages higher than about 909 kV whereas, during the tests, flashovers were observed only for voltages higher than about 960 kV. For the negative polarity, the model predicts flashovers for voltages lower than those observed in the tests for three impulses. For the 1.2/50 μs impulse (negative polarity), insulator breakdown is predicted for peak values higher than about 813 kV, against 970 kV observed in the tests. For the 2/10 μs impulse (negative polarity), the model predicts flashovers for voltages higher than about 956 kV, whereas the minimum value observed in the tests was 995 kV. For the 2.5/14 μs impulse (negative polarity), the model predicts flashover for voltages equal to or higher than 910 kV, whereas in the tests the minimum observed value was 985 kV.

Using the Hileman procedure (HILEMAN, 1999) to obtain the Integration Method parameters led to larger deviations of the measured times to breakdown compared to the proposed model. The mean and maximum differences were, respectively, 2.26 μs and 9.1 μs (1.2/50 μs impulse). For the 2.5/14 μs impulse, the procedure predicts flashovers for peak values higher than about 889 kV, whereas the minimum value observed in the tests was 960 kV. For the 2/10 μs impulse, flashovers are predicted for peak values higher than about 937 kV, whereas the minimum value observed in the tests was 970 kV. For the 1.2/6 μs impulse, flashovers are predicted for peak values higher than about 1017 kV, whereas the minimum value observed in the tests was 1070 kV. For the negative polarity, flashovers were not predicted for the lower magnitudes of the 1.2/50 μs and 2.5/14 μs impulses and for any of the test voltages of the 1.2/6 μs and 2/10 μs impulses. Note that for the 2/10 μs impulse (Fig. 24) the lowest voltage level of the Hileman's curve is above the measured curve's highest level.

In conclusion, the proposed model of the 138 kV insulator was able to predict insulator breakdown for the four impulses, of both polarities, considered in the analysis. However, for the 2.5/14 μs impulse of positive polarity and three impulses of negative polarity (1.2/50 μs, 2/10 μs and 2.5/14 μs), it predicts flashovers for voltage levels lower than those observed in the tests. The obtained results indicate that it can represent with good accuracy the insulator behavior under positive impulses, and with reasonable accuracy the behavior under negative impulses. It still exists the possibility to achieve better consistency between model and experimental results by using the modified integration method (CHOWDHURI; MISHRA; MCCONNELL, 1997,

SHIGIHARA et al., 2016, SHIGIHARA et al., 2017) using a non-constant k factor, but the model that is available in the EMTP does not allow the application of a non-constant k factor.

Considering that downward negative flashes correspond to about 90% of the cloud-to-ground flashes (CIGRE WG C4.407, 2013), the great majority of the overvoltages across the insulator terminals in the case of direct strokes to the tower or the overhead ground wires will be of positive polarity. This happens because if a negative downward flash hits the top of the tower, negative charges are injected into the tower. Therefore, the bases of the line insulators, which are connected to the tower, will be negative in relation to the phases. Thus, the voltages between the phases and the bases of the insulators will be positive. Therefore, the proposed model is suitable to estimate the occurrence of flashovers on the 138 kV insulators.

The model corresponding to the adoption of the Hileman procedure predicts flashover for voltages lower than those obtained in the tests for the 1.2/6 μs, 2.5/14 μs, and 2/10 μs impulses of positive polarity. For the negative polarity, flashovers were not predicted for the lower magnitudes of the 1.2/50 μs and 2.5/14 μs impulses and for any of the test voltages of the 1.2/6 μs and 2/10 μs impulses.

Regarding the volt-time curves of the MV line spacer of positive polarity, the Hileman procedure predicts flashovers for voltages higher than about 250 kV, whereas the minimum value observed in the tests was 262 kV. The proposed model predicts flashover for all voltage levels considered in the tests, and does not predict flashovers for voltage levels lower than those observed in the tests.

This chapter presented models for each line component: the conductors, grounding, stroke current, towers and insulators. The tower and insulator models were validated, respectively, through scale model experiments and comparisons between measured and calculated V-t curves corresponding to non-standard impulses representative of overvoltages caused by direct lightning strikes to the line towers.

3. REDUCED SCALE MODEL

A reduced scale model is a powerful tool that was very useful in the past for dealing with problems that are too complex to be solved with theory alone. The scale model technique enables tests to be performed under controlled conditions and allows for the simulation of a wide variety of situations (PIANTINI et al., 2007; PIANTINI and JANISZEWSKI, 2023).

In order to validate the computer simulations by comparing measured and calculated voltages, a 1:20 scale model of the hybrid overhead line was developed and implemented. A line section with four spans was built, as shown in Fig. 31. The line is matched at both terminations. As indicated in the figure, the current is injected into the top of the central tower. The towers are represented by 1.2 m high metal pipes. Fig. 32 shows one of the towers and the line conductors.

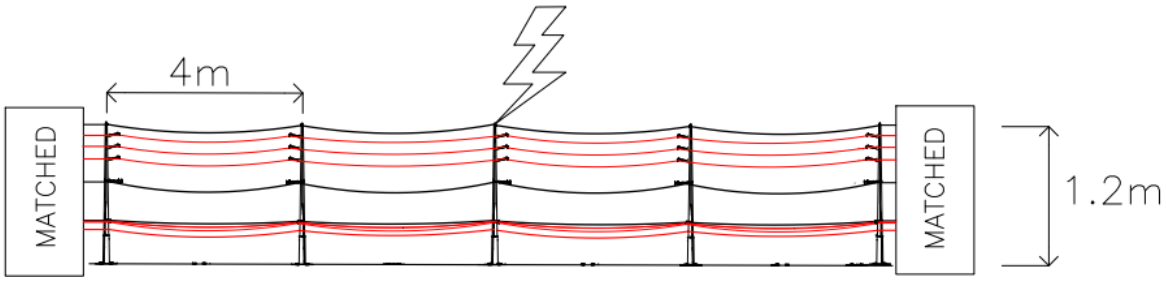

Fig. 31. 1:20 line model, matched at both terminations.

Enameled copper wires with a diameter of 0.723 mm were used for the HV and MV lines. Even though the insulation layer is very thin, the minimum impulse voltage required to cause a short circuit in case of inadvertent contact between the MV conductors is much higher than the voltages observed in the experiments. The LV line, with multiplex configuration, was simulated by copper wires with a diameter of 0.511 mm and PVC coating.

The HV insulators, made of nylon, are 7 cm long - about 20 times shorter than the 138 kV polymeric insulator mentioned in subsection 2.5.1. The spacer used in the MV line was made with a 3D printer using PLA (Polylactic Acid). The ground, simulated by interconnected aluminum plates, can be assumed as a perfectly conducting plane.

Fig. 32. Tower and line conductors (BATISTA MORAES et al., 2022).

In the experiments performed in this study, the current was injected into the line through a horizontal coaxial cable perpendicular to the line, and was measured by a Pearson current monitor model 2877. The measuring system bandwidth was from d.c. to 200 MHz.

The voltages were measured by high impedance probes with a capacitance of 11 pF and bandwidth from dc to 500 MHz. The sampling rate and bandwidth of the oscilloscope (Agilent, model DSO-X 3032A) were 2 GSamples/s and 350 MHz, respectively.

3.1. Comparisons between measured and calculated results

Tests were performed on the scaled system to enable comparisons between measured and calculated currents and voltages. Fig. 33 shows one of the currents injected into the top of the central tower; in this case the current front time is equal to 55.4 ns, which corresponds to tf = 1.1 μs for a full-scale system. The corresponding voltage at the tower top is shown in Fig. 34. The phase-to-ground voltages on phase A, phase B, underbuilt shield wire (USW) and phase D of the MV circuit (shown in Fig. 3) are depicted in Figs. 35, 36, 37, and 38, respectively. The value of the ground resistance was low, around 1 Ω.

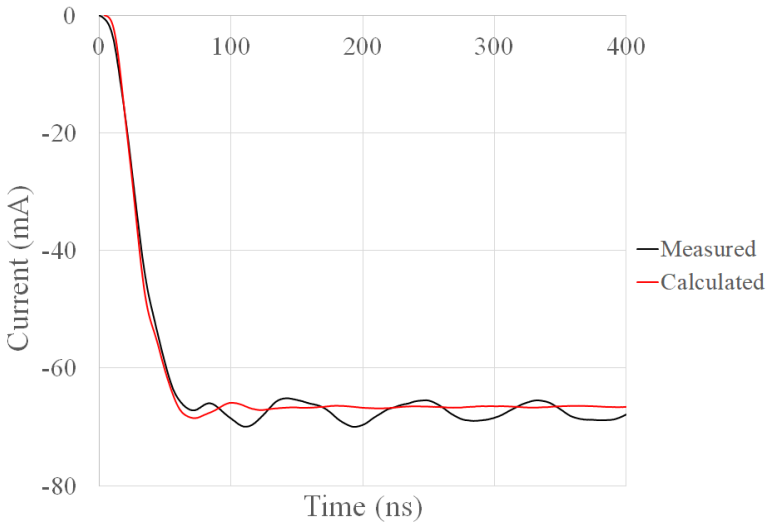

Fig. 33. Measured and calculated currents (stroke current front time tf = 55.4 ns) injected into the top of the central tower. Ground resistance = 1 Ω (PIANTINI, 2023).

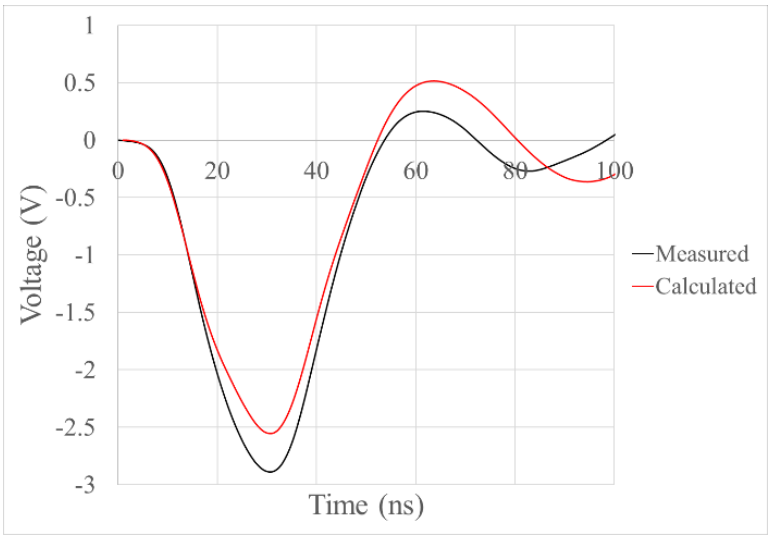

Fig. 34. Measured and calculated voltages on the top of the central tower for the current shown in Fig. 33. Ground resistance = 1 Ω, tf = 55.4 ns (PIANTINI, 2023).

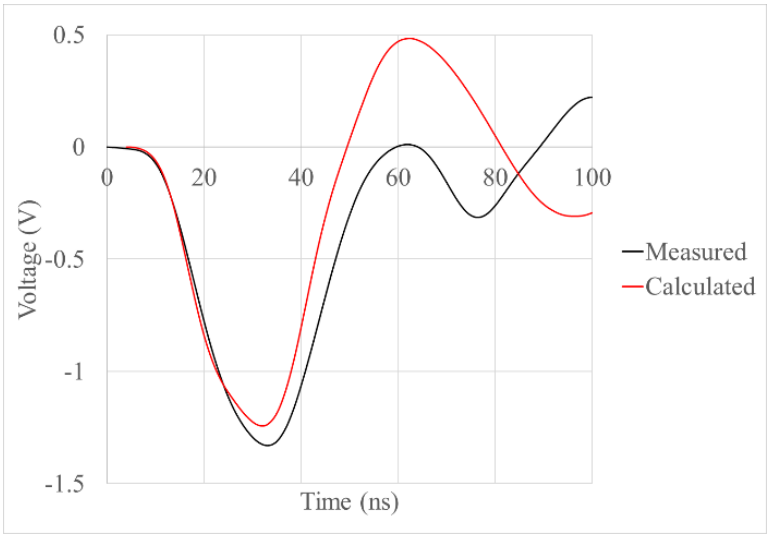

Fig. 35. Measured and calculated phase-to-ground voltages on phase A (Fig. 3) - central tower - for the current shown in Fig. 33. Ground resistance = 1 Ω, tf = 55.4 ns.

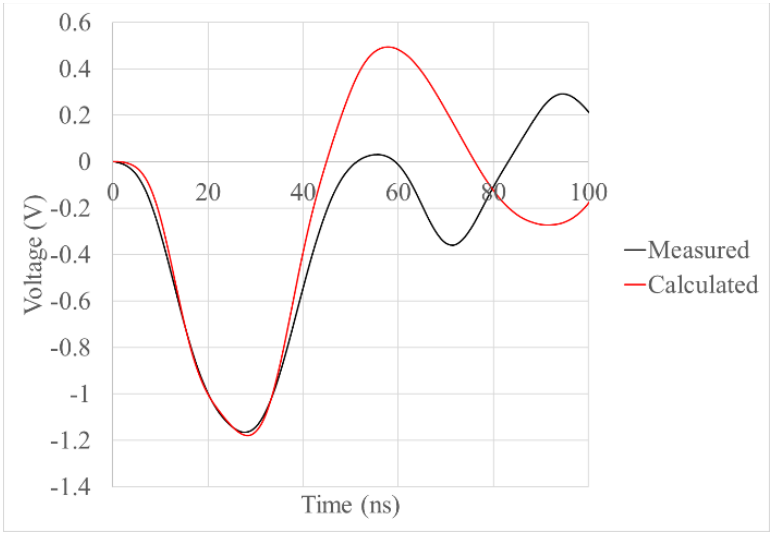

Fig. 36. Measured and calculated phase-to-ground voltages on phase B (Fig. 3) - central tower - for the current shown in Fig. 33. Ground resistance = 1 Ω, tf = 55.4 ns (PIANTINI, 2023).

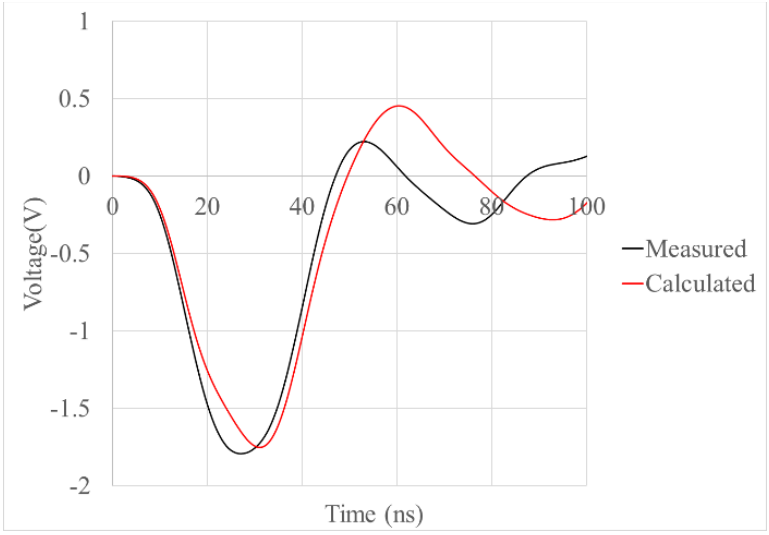

Fig. 37. Measured and calculated phase-to-ground voltages on USW (Fig. 3) - central tower - for the current shown in Fig. 33. Ground resistance = 1 Ω, tf = 55.4 ns (PIANTINI, 2023).

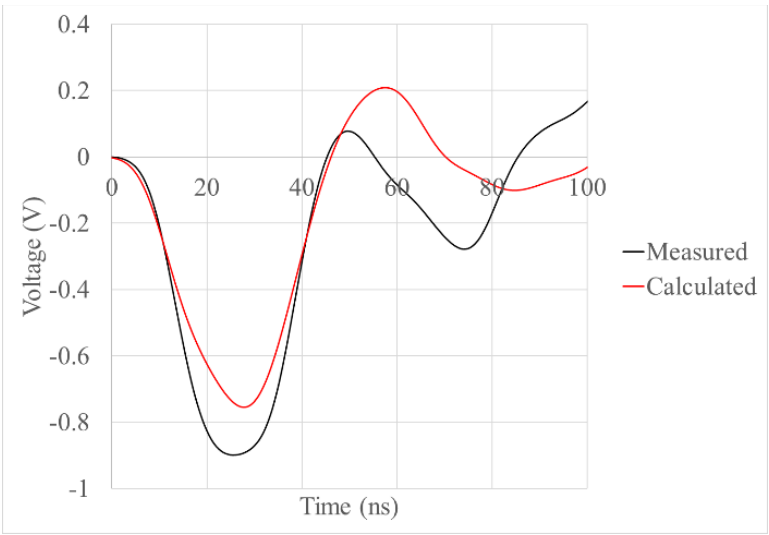

Fig. 38. Measured and calculated phase-to-ground voltages on phase D of the MV circuit (Fig. 3) - central tower - for the current shown in Fig. 33. Ground resistance = 1 Ω, tf = 55.4 ns (PIANTINI, 2023).

Both for the current and the voltages, Figs 33 to 38 show a reasonably good agreement between measured and calculated amplitudes and waveshapes. Other tests were performed, considering different current front times and observation points, and similar results were obtained.

Concerning the voltages, the agreement is reasonable, especially before about 53 ns, which corresponds to the arrival, at the observation point, of the voltages reflected at the line ends due to the imperfect matching. Possible reasons for the greater divergence at later times may be associated with inaccuracies in the models of the system components (especially the tower), whose influences tend to be more evident over time. This occurs because, subsequently, more

sections of the line affect the voltages, which are also more influenced by the reflections that occur at the various discontinuity points.

Table 10 shows the deviation of the calculated voltage peaks in relation to the measured ones for the examples shown in Figs. 34 to 38. The deviations were calculated according to (7):

$$Deviation = \left(\frac{V_{calculated} - V_{measured}}{V_{measured}}\right).100\% \quad (7)$$

Table 10 - Deviations of the calculated voltage peaks in relation to the measured ones.

	Vtop	**Phase A**	**Phase B**	**USW**	**Phase D (MV circuit)**
Deviation (%)	-11.6	-6.6	1.2	-2.3	-16.0

The deviations vary from 1.2% to 16% in terms of absolute values, as range that can be considered satisfactory for the purposes of this study.

3.2. Summary

In Chapter 3, a reduced scale model of a hybrid overhead line with four spans and matched at both terminations was developed and deployed. Currents were injected at the top of the central tower and voltages were measured at different points: tower top, phase A and phase B of the HV Line, USW, and phase D of the MV circuit (Fig. 3). Comparisons between measured and calculated results were performed.

The deviations between the measured and calculated absolute values of the peak voltages varied in a range from 1.2% to 16%. The results indicate the adequacy of the models used in both the EMTP simulations and in the reduced scale system for investigating overvoltages in hybrid overhead lines.

4. INFLUENCES OF VARIOUS PARAMETERS ON THE OVERVOLTAGES CAUSED BY DIRECT LIGHTNING STRIKES

This section presents analyses of the influences of various parameters on the overvoltages caused by direct lightning strikes to the hybrid overhead line shown in Fig. 2 and Fig. 3.

For a stroke current representing a typical first stroke current of a negative downward flash with a peak value of 31 kA injected into the top of the central tower, voltages are computed between phase D (Fig. 3) and the ground, as well as between phase D and the messenger of the MV circuit. Phase D tends to exhibit higher voltages with respect to the other phase conductors of the MV circuit because it is located farthest from the messenger and, therefore, the coupling effect is weaker.

A single parameter was varied at a time to evaluate its individual impact. Therefore, unless otherwise indicated, the parameters adopted in the simulations are those assumed for the base case: impulse impedance of the grounding system (Zg) equal to 20 Ω, soil resistivity equal to 1000 Ωm, conductors' d.c. resistances as indicated in Table 1, stroke current front time of 3.8 μs, insulator capacitance of 75 pF, and tower impulse impedance of 297 Ω. The lightning channel impedance is assumed to be infinite, and the conductors' sag are not considered in the base case.

4.1. Ground impulse impedance and soil resistivity

Fig. 39 shows the voltages between phase D and the ground and between phase D and the messenger for impulsive impedance Zg = 20 Ω and the following values for the soil resistivity: 100 Ωm, 500 Ωm, 1000 Ωm, 2000 Ωm, and 4000 Ωm.

The magnitudes of the phase-to-ground voltages increase with the soil resistivity. By varying the soil resistivity from 100 Ωm to 4000 Ωm, the absolute value of the peak voltage between phase D and the ground increases by 25%. Conversely, the voltage between phase D and the

messenger has an inverse behavior, showing a decrease of approximately 23% for the same variation of the soil resistivity.

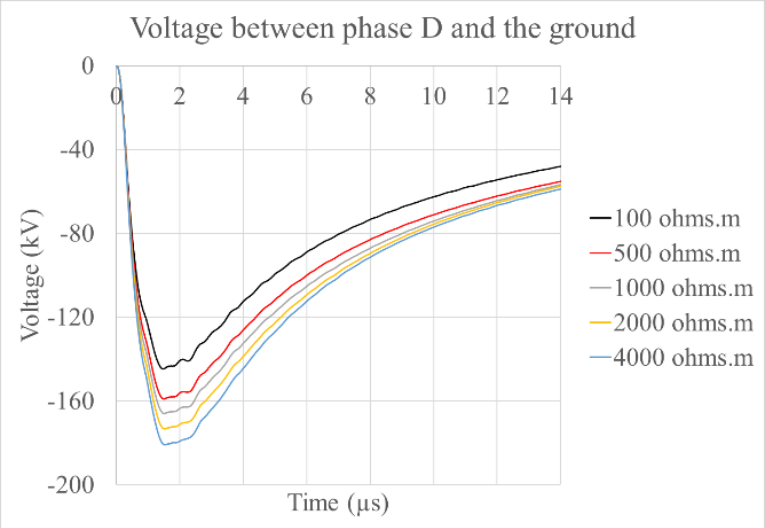

(a)

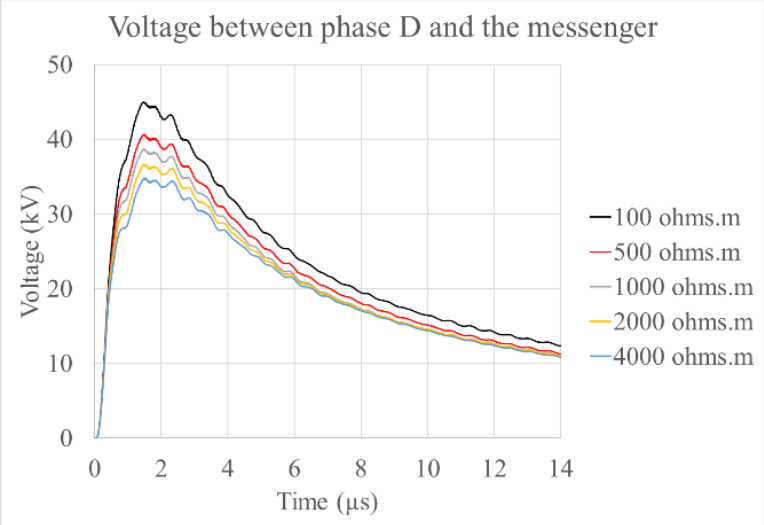

(b)

Fig. 39. Voltages on phase D (Fig. 3) for Zg = 20 Ω and different soil resistivity values (BATISTA MORAES et al., 2023).
a) Phase-to-ground b) Phase-to-messenger

High soil resistivity contributes to amplify the voltage magnitudes in all conductors. However, the variations of the messenger voltage (which has higher absolute value than the voltage on phase D) are smaller in comparison with those in phase D, causing a decrease in the voltage

difference between phase D and the messenger. With a transition from 100 Ωm to 4000 Ωm soil resistivity, phase D voltage magnitude varies from about - 145 kV to - 181 kV (25% variation). The corresponding messenger-to-ground voltage magnitude shifts from about - 190 kV to - 216 kV (with an approximate 14% increase).

Fig. 40 shows the voltages between phase D and the ground and between phase D and the messenger for the soil resistivity of 1000 Ωm and adopting various impulse impedance values for the grounding system: 5 Ω, 10 Ω, 20 Ω, 40 Ω, and 80 Ω. With an increase of the impulse impedance, the absolute value of the voltage between phase D and the ground increases. The comparison between Fig. 39(a) and Fig. 40(a) shows that the influence of the impulse impedance is more significant than that of the soil resistivity. Increasing Zg from 5 Ω to 80 Ω leads to an increase of approximately 247% in the voltage between phase D and the ground.

Unlike the previous case (Fig. 39b), the voltage between phase D and the messenger increases with the increase of the impulse impedance value. For the same variation in Zg, the phase D voltage peak varies from - 98 kV to - 341 kV (corresponding to a variation of 247%). The corresponding peak voltage shift between the messenger and the ground is from - 115 kV to - 434 kV (variation of 277%). This results in an increase of approximately 400% in the voltage difference between phase D and the messenger.

The ranges of values for soil resistivity and Zg have been chosen to illustrate the significant sensitivity of the calculated overvoltages. While all combinations of values are realistic, extreme cases, such as the combination of 4000 Ωm soil resistivity with Zg = 20 Ω and 1000 Ωm soil resistivity with Zg = 5 Ω, would likely not be economically justified for the specific line considered in this thesis.

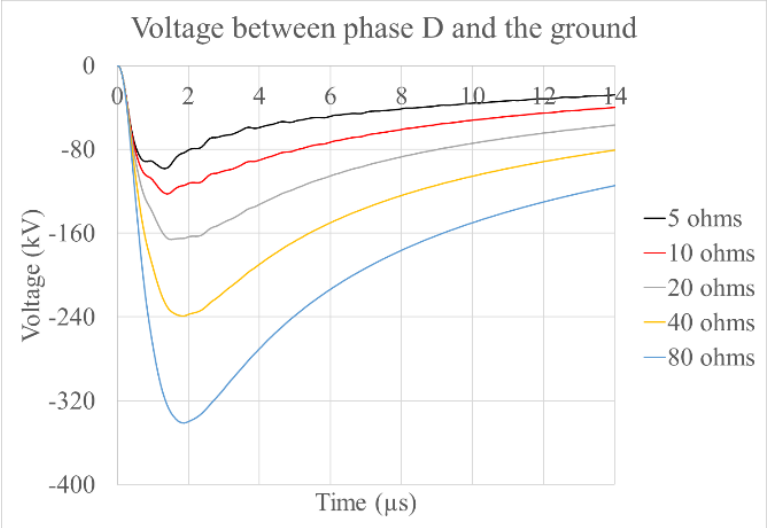

(a)

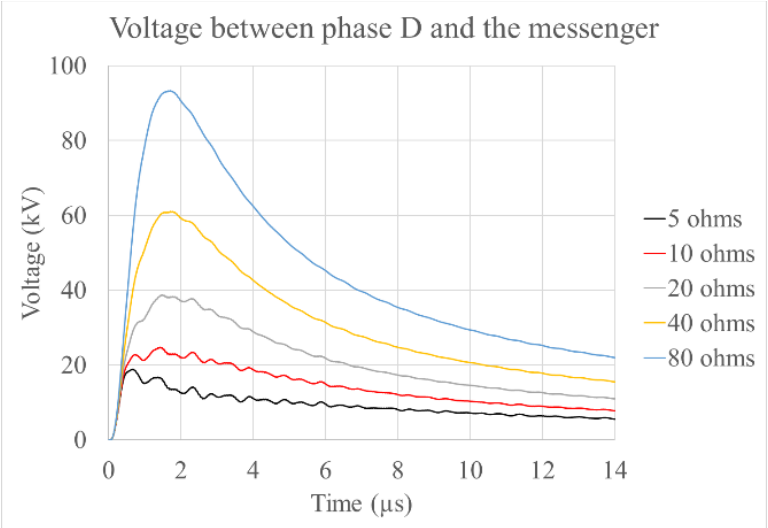

(b)

Fig. 40. Voltages on phase D (Fig. 3) for ρ = 1000 Ωm and different ground impulse impedance values (BATISTA MORAES et al., 2023).
a) Phase-to-ground b) Phase-to-messenger

4.2. Conductors d.c. resistances

In the literature on the subject, the d.c. resistances of the conductors are sometimes disregarded. Therefore, it is worthwhile to investigate how they affect the voltages between phase D and the ground and between phase D and the messenger. Fig. 41 illustrates such influence using the resistance values indicated in Table 1.

Fig. 41 shows the influence of the d.c. resistances of the conductors on the voltages between phase D and the ground and between phase D and the messenger. When the d.c. resistances are considered, the absolute value of the voltage between phase D and the ground increases, while there is a converse trend in the voltage between phase D and the messenger.

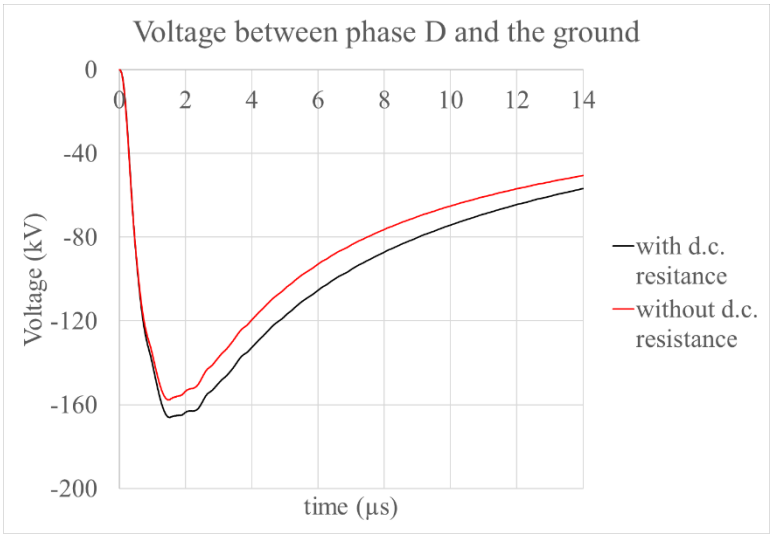

(a)

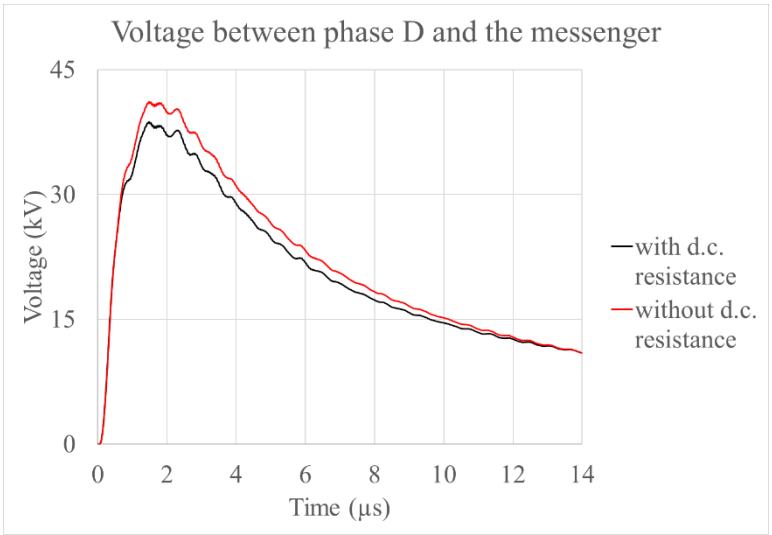

(b)

Fig. 41. Voltages on phase D (Fig. 3) for ρ = 1000 Ωm and Zg = 20 Ω, considering or not the conductors' d.c. resistances (BATISTA MORAES et al., 2023).
a) Phase-to-ground b) Phase-to-messenger

The conductors' resistances, while causing an increase in the voltages on all conductors, have a more pronounced impact on phase D than on the messenger. The voltage absolute value

between phase D and the ground increases by approximately 5% (shifting from about 158 kV to 166 kV), while between the messenger and the ground there is a roughly 3% enhancement (from 199 kV to 205 kV). The voltage magnitude between phase D and the messenger decreases by approximately 5% (from about 41 kV to 39 kV).

4.3. Lightning channel impedance

The influence of the value of the channel impedance on the voltages between phase D and the ground and between phase D and the messenger is illustrated in Fig. 42. The considered values of the channel impedance are infinite, 1000 Ω, and 500 Ω. The results show the negligible influence of the channel impedance for the considered study case. Specifically, the ratio of the peak values of the voltages corresponding to channel impedance equal to infinite and 500 Ω is 1.02 both for the voltage between phase D and the ground (which varies from 164 kV to 166 kV) and for the voltage between phase D and the messenger (ranging from 38 kV to 39 kV).

It is important to stress that the simulations shown in Fig. 42 refer to a ground impulse impedance of 20 Ω. However, in the case of high ground impulse impedance values, the influence of the channel impedance might not be negligible, as shown by (DATSIOS; MIKROPOULOS; TSOVILIS, 2019).

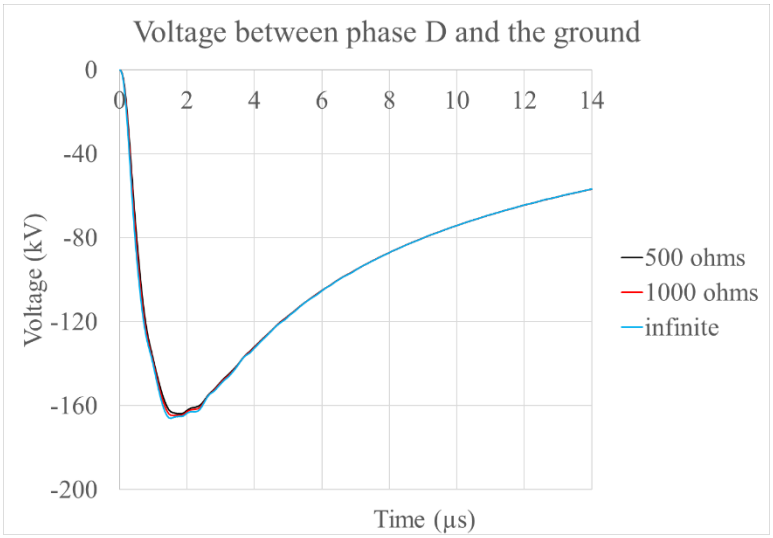

(a)

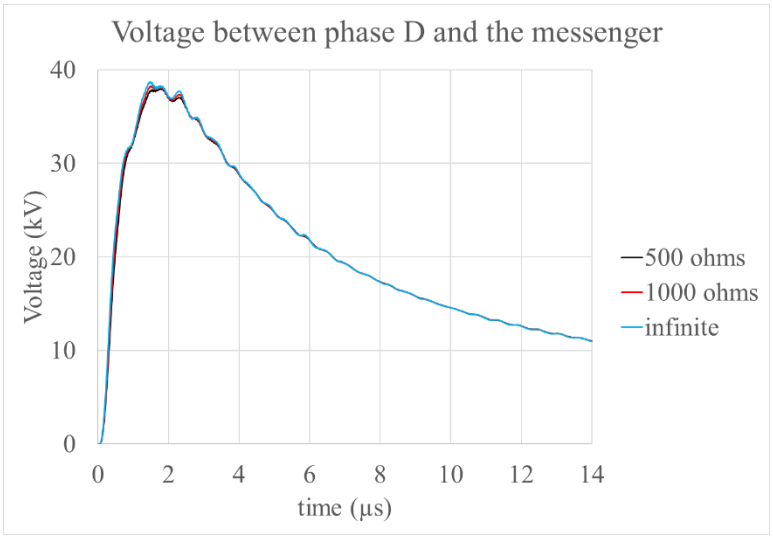

(b)

Fig. 42. Voltages on phase D (Fig. 3) for ρ =1000 Ωm, Zg = 20 Ω, and different channel impedance values (BATISTA MORAES et al., 2023).
a) Phase-to-ground b) Phase-to-messenger

4.4. Stroke current front time (tf30-90)

Fig. 43 shows the voltages between phase D and the ground and between phase D and the messenger for stroke current front times of 1 µs, 2 µs, 3.8 µs, and 8 µs. The influence of the current front time is significant. The longer the front time, the lower the voltage peak value for both voltages. When the current front time increases from 1 µs to 8 µs, the absolute value of the peak voltage between phase D and the ground decreases by approximately 75% (from - 496 kV to -121 kV), while the peak value of the voltage between phase D and the messenger decreases approximately 80% (from about 150 kV to 27 kV).

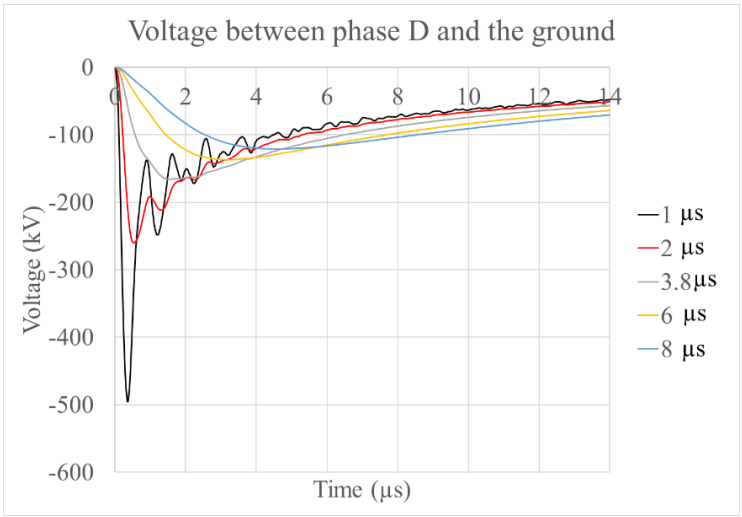

(a)

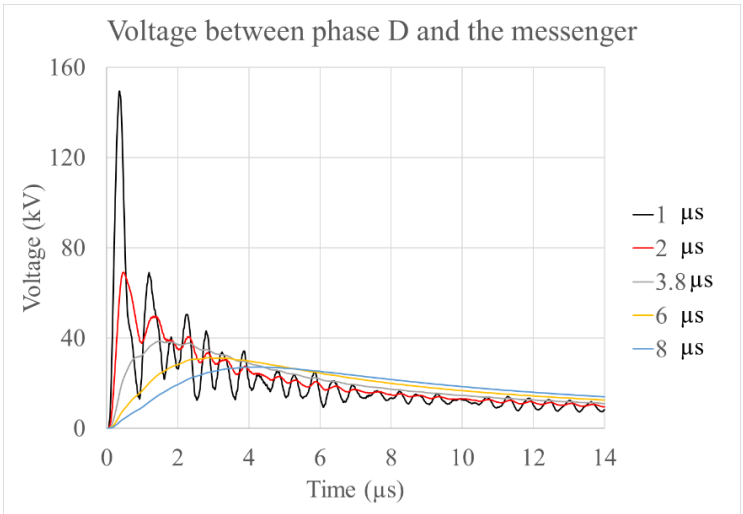

(b)

Fig. 43. Voltages on phase D (Fig. 3) for ρ =1000 Ωm, Zg = 20 Ω, and different stroke current front times (BATISTA MORAES et al., 2023).
a) Phase-to-ground b) Phase-to-messenger

4.5. Insulator capacitance

The influence of the HV insulator capacitance on the voltages between phase D and ground and between phase D and messenger is illustrated in Fig. 44 for capacitances of 0 pF, 75 pF, and 150 pF. This influence is negligible on both voltages. The ratios between the peak values of the voltages corresponding to the cases of capacitances equal to 0 pF and 150 pF are 0.997 (from - 165.6 kV to -166.2 kV) for the voltage between phase D and ground and 1.003 (from 38.7 kV to 38.6 kV) for the voltage between phase D and the messenger.

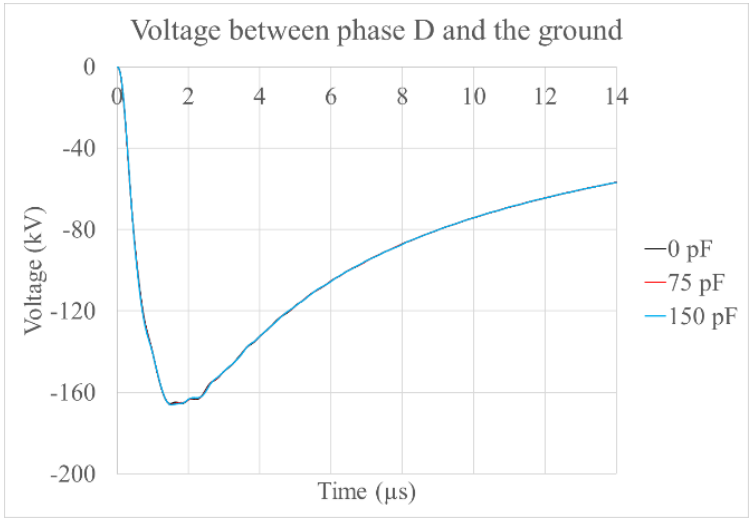

(a)

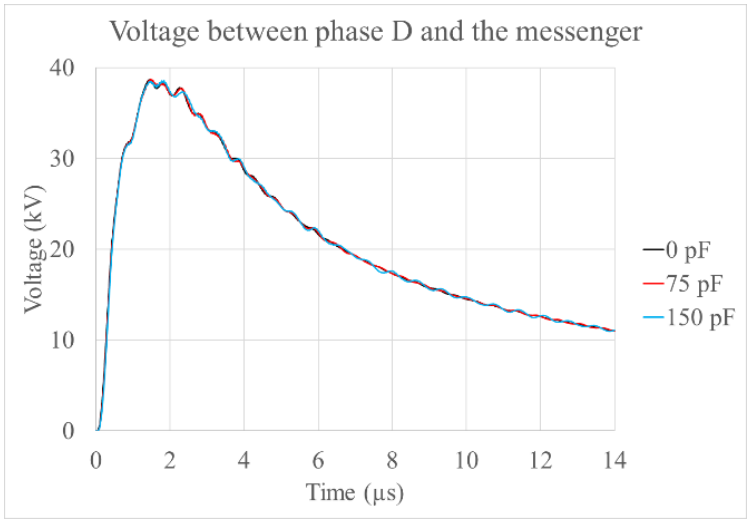

(b)

Fig. 44. Voltages on phase D (Fig. 3) for ρ = 1000 Ωm, Zg = 20 Ω, and different HV insulator capacitances (BATISTA MORAES et al., 2023).
a) Phase-to-ground b) Phase-to-messenger

4.6. Conductors' sag

Fig. 45 illustrates the influence of the conductors' sag on the voltages between phase D and the ground and between phase D and the messenger. The conductors' heights at the tower and the middle of the span are indicated in Table 11. They correspond to the heights measured in the 1:20 line model built in the laboratory multiplied by 20 to represent a full-scale line. Fig. 45 indicates that the influence of conductors' sag on both voltages is negligible. The ratio of the peak voltage values, when considering the presence or absence of conductors' sag, reaches the value of 1.001 for the voltage between phase D and the ground (varying from - 166.3 kV to - 166.1 kV) and 0.99 for the voltage between phase D and the messenger (varying from 38.4 kV to 38.7 kV).

Table 11 - Conductors' heights at the tower and middle of the span.

Conductor	Height at the tower (m)	Height at the middle of the span (m)
OHGW	24	21.7
Phase A	22	18.75
Phase B	20	16.3
Phase C	18	13.55
USW	15	11.1
Messenger	9.3	7
Phase R (MV)	9.175	6.88
Phase D (MV)	9	6.7
Phase L (MV)	9.175	6.88
Neutral	8	6
Phase r (LV)	7.78	5.98
Phase d (LV)	7.76	5.96
Phase l (LV)	7.78	5.98

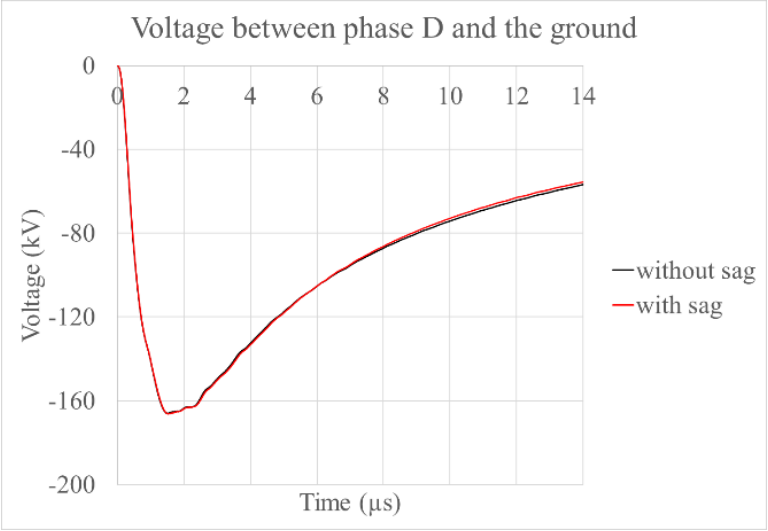

(a)

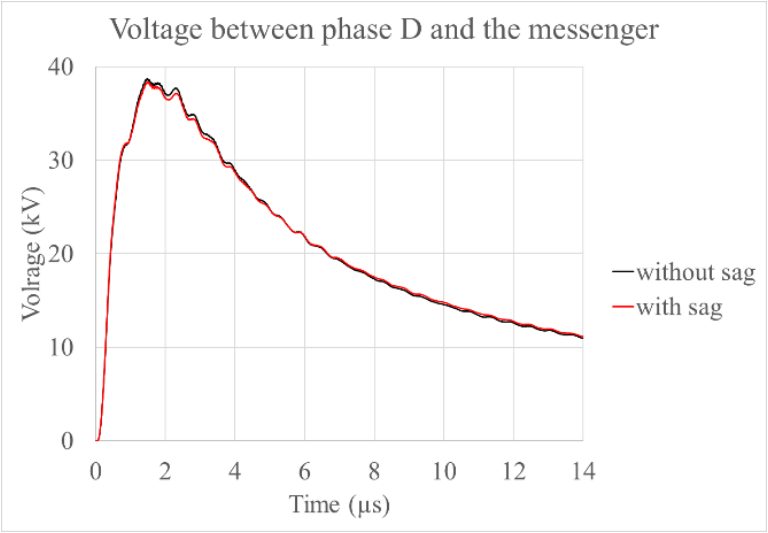

(b)

Fig. 45. Voltages on phase D (Fig. 3) for ρ =1000 Ωm and Zg = 20 Ω considering and not considering the conductors' sag (BATISTA MORAES et al., 2023).
a) Phase-to-ground b) Phase-to-messenger

4.7. Tower surge impedance

In order to illustrate the effect of the tower surge impedance, Fig. 46 shows the voltages between phase D and the ground and between phase D and the messenger for a range of tower impedance values: 100 Ω, 200 Ω, 300 Ω, 400 Ω, and 600 Ω.

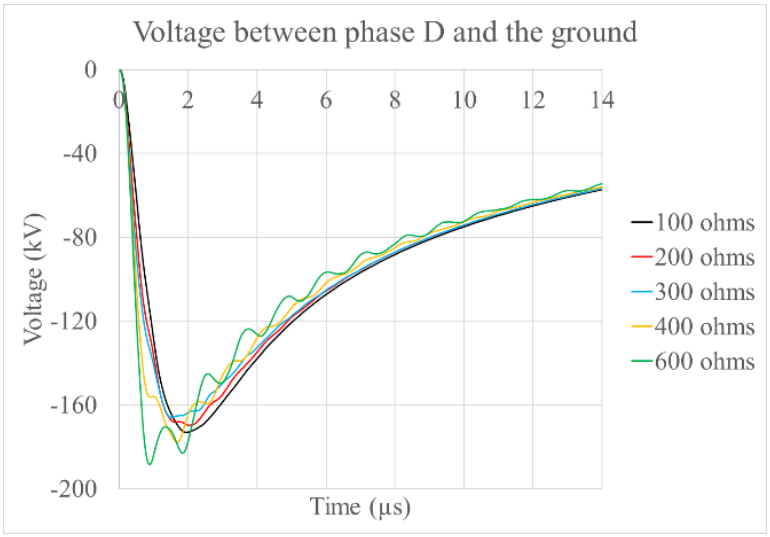

(a)

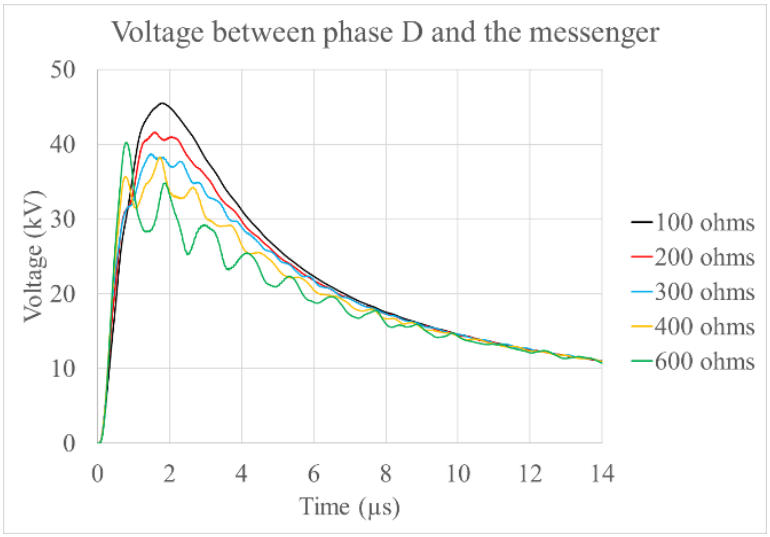

(b)

Fig. 46. Voltages on phase D (Fig. 3) for ρ =1000 Ωm and Zg = 20 Ω and different tower impulse impedance values (BATISTA MORAES et al., 2023).

a) Phase-to-ground b) Phase-to-messenger

The results shown in Fig. 46 indicate that when the surge impedance increases from 100 Ω to 300 Ω, the absolute value of the voltage between phase D and the ground decreases 4% and the voltage between phase D and the messenger decreases about 15%. When the surge impedance increases from 300 Ω to 600 Ω, the phase-to-ground voltage increases 13.4% (absolute values) and the phase-to-messenger voltage increases 4%.

The analysis of the effect is not so simple because the voltages on phase D are affected by the voltages reflected at the tower base and by the currents injected into the grounded conductors,

especially into the messenger. Depending on the conditions, these effects may be opposite concerning the tower surge impedance.

Since, in general, the ground impulse impedance (Zp) is smaller than the tower surge impedance (Z_T), the voltage reflected at the tower base has opposite polarity with respect to the incoming voltage and arrives at the calculated point (phase D) before the voltage (at phase D) reaches its peak, the higher the absolute value of the reflected voltage, the lower the absolute value of the voltage at the observation point.

The voltage reflected at the tower base depends on the magnitude of the current that flows to the tower base and on the reflection coefficient. Its absolute value increases with the magnitude of the current that flows to the tower base and the absolute value of the reflection coefficient. The former decreases with the increase of Z_T, whereas the latter depends on the values of Z_T and the ground impulse impedance (Zp). For the low value assumed for Zp (20 Ω), the absolute value of the reflection coefficient increases with Z_T. Therefore, the reflected voltage may increase or decrease with Z_T, depending on the case.

Regarding the messenger, the larger the magnitude of the current injected into it, the more significant the contribution of this current to decrease the voltage amplitude on phase D. The greater the tower impedance, the greater the portion of the current injected into the messenger (relatively to the current injected into the ground through the tower base) in the initial instants (up to about 1.5 μs). As a result, the contribution of this current to lowering the voltage magnitude on phase D becomes more significant.

Hence, depending on the combination of the values of parameters such as the ground impulse impedance, tower surge impedance, impedance of the conductors, and stroke current front time, increasing Z_T can cause either an increase or a decrease in the voltage between phase D and the ground.

Fig. 46a shows that, for the considered situations, the effect of the current through the messenger dominates over that of the current at the tower bottom for Z_T in the range of 100 Ω to about 300 Ω, and the absolute value of the voltage between phase D and the ground decreases with Z_T. For Z_T higher than 300 Ω, the situation is reversed, and the absolute value of the voltage increases as Z_T increases.

Regarding the voltage between phase D and the messenger, one should note that the absolute value of the voltage between the messenger and the ground tends to increase with Z_T since, in this condition, a higher current is injected into the conductor. The variation of the voltage on

the messenger is more significant than that on phase D. Fig. 46b shows that the voltage tends to decrease with the tower impedance, but when Z_T is increased from 400 Ω to 600 Ω, the voltage peak increases slightly.

5. CRITICAL CURRENTS

The critical current is the minimum lightning stroke current that would cause a line flashover (IEEE, 2011). In this section, the critical currents for the case of lightning hitting the line's central tower are calculated for the first and subsequent stroke currents represented by Heidler functions with the parameters indicated in Table 12, that is, the front time dependence on the current amplitude was not considered. The parameters shown in Table 12 can be considered typical of lightning currents with magnitudes corresponding to the probability of approximately 50% of being exceeded (IEEE, 2011), namely 31 kA for the first and 12 kA for the subsequent stroke. The steady-state AC voltage was not taken into account.

Table 12 - Parameters of the Heidler function (HEIDLER; CVETIĆ, 2002) for the first and subsequent stroke currents.

First Stroke				Subsequent Stroke							
I_0(kA)	τ_1 (μs)	τ_2 (μs)	n	I_{01}(kA)	τ_{11} (μs)	τ_{21} (μs)	n_1	I_{02}(kA)	τ_{12} (μs)	τ_{22} (μs)	n_2
29.3	1.44	91.8	2	10.7	0.25	2.5	2	6.5	2.1	230	2

Actually, the lightning performance of the MV line is related to both direct and indirect strokes. However, for the line under study, the number of overvoltages associated with indirect strokes is much lower than that caused by direct strokes. BORGHETTI et al. (2020) compared the number of direct and indirect events/100 km/year exceeding 150 kV and 300 kV in the MV line of the same system considered in this dissertation. The soil resistivity was equal to 1000 Ωm, and two values were considered for the ground resistance (20 Ω and 40 Ω), which was implicitly regarded as equal to the ground impulse impedance. The authors also considered the case of surge arresters installed every four or eight poles in the MV line.

Table 13 presents the results for the case of an unprotected line, i.e., a line without arresters, which corresponds to the same configuration discussed in this dissertation. The number of overvoltages caused by direct strokes is significantly higher than that due to indirect strokes. It is also clear that the impact of the indirect strokes on the lightning performance of the MV line

decreases with the increase of both the CFO and the ground impedance. Similar results were obtained by BORGHETTI et al. (2020) for a hybrid overhead line with a 69 kV HV circuit.

Although different models were adopted by BORGHETTI et al. (2020) for simulating the line conductors, tower, and HV insulators, it can be assumed that the same conclusion regarding the impact of the indirect strokes on the lightning performance of the MV line would be obtained with the use of the models developed and adopted in this dissertation.

Table 13 - Number of direct (N_d) or indirect (N_i) events/100 km/year exceeding voltage W in the MV line for different values of the ground resistance. Adapted from BORGHETTI et al. (2020).

Ground resistance	**W = 150 kV**		**W = 300 kV**	
	N_d	**N_i**	**N_d**	**N_i**
20 Ω	7.6	0.3	1.4	$< 10^{-2}$
40 Ω	11.0	0.2	2.8	$< 10^{-2}$

In this chapter, the simulations to obtain the critical currents are performed assuming the following pairs of soil resistivity and ground impulse impedance values: 500 Ωm – 10 Ω, 1000 Ωm – 20 Ω, 2000 Ωm – 40 Ω, and 4000 Ωm - 80 Ω. The lightning channel impedance is equal to infinite, the conductors' d.c. resistances are those shown in Table 1, the conductors heights are assumed constant and equal to the heights at the tower (Table 11), and the insulators are modeled as described in subsection 2.5.

The calculated critical currents are presented in Table 14 for the HV and MV circuits. The probabilities of the values of the critical currents to be exceeded, calculated according to the IEEE approximation (IEEE, 2011) and indicated by (8) and (9), are also shown. As the IEEE approximation may not apply to first stroke currents surpassing 200 kA, these specific instances are indicated in bold font in the table, as well as those of critical subsequent stroke currents higher than 100 kA.

$$P(I \geq i_0) = \frac{1}{1+\left(\frac{i_0}{31}\right)^{2.6}} \tag{8}$$

where $P(I \geq i_0)$ is the probability that the first return stroke has a peak current Io that exceeds i_0 and i_0 is the prospective first return stroke peak current (kA).

$$P(I \geq i_0) = \frac{1}{1+\left(\frac{i_0}{12}\right)^{2.7}} \quad (9)$$

where $P(I \geq i_0)$ is the probability that a subsequent return stroke has a peak current Io that exceeds i_0, and i_0 is the prospective subsequent return stroke peak current (kA).

Table 14 - Critical currents and their corresponding probabilities of being exceeded for the first (I_{FS}) and subsequent (I_{SS}) strokes and HV and MV line circuits.

Line circuit		Soil resistivity – Ground impulse impedance			
		500 Ωm - 10 Ω	1000 Ωm - 20 Ω	2000 Ωm - 40 Ω	4000 Ωm - 80 Ω
HV	I_{FS}	**371 kA (0.16%)**	**318 kA (0.23%)**	**258 kA (0.40%)**	**201 kA (0.77%)**
	I_{SS}	**131 kA (0.16%)**	**126 kA (0.17%)**	**119 kA (0.20%)**	**107 kA (0.27%)**
MV	I_{FS}	**437 kA (0.10%)**	**280 kA (0.33%)**	191 kA (0.88%)	131 kA (2.3%)
	I_{SS}	**222 kA (0.038%)**	**183 kA (0.064%)**	**130 kA (0.16%)**	89 kA (0.45%)

As shown in Table 14, the critical currents decrease as the ground impulse impedance increases. Moreover, the first stroke current is more severe than the subsequent stroke current. The critical currents are high for both HV and MV circuits, which attests the excellent lightning performance of the line even for the most challenging conditions considered. In fact, it is improbable that a subsequent stroke may cause a backflashover in any of the circuits.

For the HV line, the probability of the critical current being exceeded varies in the range from 0.16% to 0.77%, whereas the corresponding range for the MV circuit spans from 0.10% to 2.3%. The good performance is due to the presence of the four grounded conductors (OHGW, USW, messenger, and the neutral of the LV circuit), which have collectively lower total surge impedance and a higher coupling coefficient to the phases compared to a single OHGW, thus reducing the voltages across the insulators.

Despite the MV circuit's much lower lightning withstand capability compared to the HV circuit, the presence of the four grounded conductors, together with the strong coupling between phases and messenger due to their close spacing in the adopted spacer-cable configuration, leads to a

significant reduction of the overvoltages across the spacers. This phenomenon is accentuated in extreme cases, where critical currents for the MV circuit can even surpass those of the HV circuit. This is the case of the 500 Ωm – 10 Ω combination, for which the critical currents for both the first and subsequent strokes are higher than those of the HV circuit. The critical subsequent stroke current for the MV circuit is also higher for the 1000 Ωm – 20 Ω and 2000 Ωm – 40 Ω combinations. However, the probability of stroke currents exceeding critical values in such conditions is extremely low.

It is important to note that for cases in which the MV critical currents exceed the HV critical currents, the HV insulators flash over before the MV insulators. When the critical currents for the HV circuit are higher than those of the MV circuit, flashovers occur first on the MV circuit.

As mentioned in subsection 2.5, a 100 kV increase was applied to each point of the V-t curve of the MV insulators to account for the influence of the XLPE coverage of the spacer cable. In order to evaluate the impact of such value, a supplementary analysis was carried out considering the case of adding only 50 kV to each point of the V-t curve. The results are summarized in Table 15, compared to those obtained with the original assumption. Although not realistic for the spacer cable configuration, bare conductors are considered for comparison purposes.

Table 15 - Critical currents (MV circuit) and their corresponding probabilities of being exceeded, considering different voltage values added to the V-t curves of the MV insulators.

Critical current	**Voltage added to the V-t curves**	**Soil resistivity – Ground impulse impedance**			
		500 Ωm - 10 Ω	1000 Ωm - 20 Ω	2000 Ωm - 40 Ω	4000 Ωm - 80 Ω
I_{FS}	100 kV	**437 kA (0.10%)**	**280 kA (0.33%)**	191 kA (0.88%)	131 kA (2.3%)
	50 kV	**330 kA (0.21%)**	**226 kA (0.57%)**	154 kA (1.53%)	106 kA (3.9%)
	0 kV (bare conductors)	**266 kA (0.37%)**	183 kA (0.98%)	126 kA (2.54%)	86 kA (6.6%)
I_{SS}	100 kV	**222 kA (0.038%)**	**183 kA (0.064%)**	**130 kA (0.16%)**	89 kA (0.45%)
	50 kV	**164 kA (0.086%)**	**144 kA (0.12%)**	**103 kA (0.3%)**	73 kA (0.76%)
	0 kV (bare conductors)	**156 kA (0.098%)**	**131 kA (0.16%)**	97 kA (0.35%)	68 kA (0.92%)

In terms of the critical current magnitude, the influence of varying the voltage increase applied to the MV insulator V-t curve is particularly significant in cases of low ground impulse impedance values. Illustratively, for the 500 Ωm – 10 Ω combination, the critical first stroke current has a 171 kA increase (from 266 kA to 437 kA) when the added voltage increases from 0 kV (bare conductors) to 100 kV. For the 4000 Ωm – 80 Ω combination, the corresponding increase in the critical current value amounts to 45 kA (from 86 kA to 131 kA). Conversely, the differences in the probabilities of these currents being exceeded tend to be more significant for larger values of the impulse impedance. For instance, the differences are about 0.27% (from 0.37% to 0.10%) and 4.3% (from 6.6% to 2.3%) for the combinations 500 Ωm – 10 Ω and 4000 Ωm – 80 Ω, respectively.

The same trend is observed for the critical subsequent stroke current. The increase of the added voltage value from 0 kV (bare conductors) to 100 kV causes an increase of 66 kA (from 156 kA to 222 kA) for the 500 Ωm – 10 Ω combination, and of 21 kA (from 68 kA to 89 kA) for the 4000 Ωm – 80 Ω combination. In terms of the probabilities of these critical currents being exceeded, the absolute differences are 0.06% (decreasing from 0.098% to 0.038%) for the 500 Ωm – 10 Ω combination, and 0.47% (decreasing from 0.92% to 0.45%) for the 4000 Ωm – 80 Ω combination.

Previous investigations have already shown the enhanced lightning performance of the MV circuit within a hybrid overhead line in comparison to a MV line alone (BORGHETTI et al., 2018b, 2019b, 2020; PIANTINI, BORGHETTI, NUCCI, 2020). The comparisons shown in Table 15 indicate that the lightning performance of the MV line remains very good even in adverse conditions and considering a relatively modest increase (50 kV) in its lightning withstand capability attributed to the XLPE coverage of the spacer cable.

6. CONCLUSIONS

The continuous population growth in large cities has become an obstacle in the construction of new distribution lines due to the limitations of available space. The construction of hybrid overhead lines has great potential to solve this issue and also reducing costs associated with novel power distribution infrastructure by benefitting from the operational integration of existing sub-transmission lines. However, despite these advantages, few studies have been devoted to the lightning performance analysis of this type of line.

Since lightning is one of the primary origins of overvoltages and outages in both sub-transmission and distribution lines, it is important to verify how sharing the same structures by HV and MV lines would impact the lightning performance of the distribution line.

The analyses were carried out through computer simulations, using the EMTP software, and experimental studies. All the system components were represented by reliable models in the simulations. In particular, tower and HV insulator models were developed based on comparisons involving tests carried out in the High Voltage and the Scale Model laboratories of the Institute of Energy and Environment of the University of São Paulo. The simulations considered realistic situations and indicated the adequacy of the proposed models.

A reduced scale model of a hybrid overhead line with four spans and matched at both terminations was developed and deployed. Currents were injected at the top of the central tower and voltages were measured at different points along the tower and also on the HV and MV circuits. Comparisons between measured and calculated results were performed on this type of line for the first time. The deviations between the measured and calculated absolute values of the peak voltages varied in a range from 1.2% to 16%. The results indicated the adequacy of the models used in the EMTP simulations and the reduced scale system for investigating overvoltages in hybrid overhead lines.

As the magnitude and waveform of the lightning overvoltages depend on the stroke current, network configuration, and soil characteristics, knowing how the main parameters affect the overvoltages is of great importance to evaluate the lightning performance of a hybrid overhead line. In this dissertation, the overvoltages on the medium voltage circuit of an actual hybrid overhead line due to direct lightning strikes were assessed and the effects of the main parameters

were evaluated. The main conclusions are as follows:

- the variations of the lightning channel impedance, insulator capacitance, and conductors' sag have negligible influences on the phase-to-ground and phase-to-messenger voltages;
- the magnitudes of the phase-to-ground voltages increase with the soil resistivity. By varying the soil resistivity from 100 Ωm to 4000 Ωm, the absolute value of the peak voltage between phase D and the ground increases by 25%. Conversely, the voltage between phase D and the messenger has an inverse behavior, showing a decrease of approximately 23% for the same variation;
- the absolute values of both the voltage between phase D and the ground and the voltage between phase D and the messenger increase with the impulse impedance. The influence of the impulse impedance is more significant than that of the soil resistivity. An increase in the impulse impedance from 5 Ω to 80 Ω leads to increases of approximately 247% in the phase-to-ground and 400% in the phase-to-messenger voltages;
- the absolute values of the phase-to-ground voltages increase when the conductors' d.c. resistances are considered, while there is a converse trend in the phase-to-messenger voltages. The conductors' resistances, while causing an increase in the voltages on all conductors, have a more pronounced impact on the phase voltages than on the messenger, causing the phase-to-messenger voltages to decrease. In comparison with the case of ideal conductors, the influence of the d.c. resistances, on both voltages, is of the order of 5%;
- the influence of the current front time is significant. The longer the front time, the lower the voltage peak value for both the phase-to-ground and phase-to-messenger voltages. When the current front time increases from 1 μs to 8 μs, the absolute value of the peak voltage between phase D and the ground decreases by approximately 75%, while the peak value of the voltage between phase D and the messenger decreases approximately 80%;
- the absolute values of both voltages tend to decrease initially with the increase of the tower surge impedance, but above a certain critical value they start to increase. When the surge impedance increases from 100 Ω to 300 Ω, the absolute value of the voltage between phase D and the ground decreases 4% and the voltage between phase D and

the messenger decreases about 15%. When the surge impedance increases from 300 Ω to 600 Ω, the phase-to-ground voltage increases 13.4% (absolute values) and the phase-to-messenger voltage increases 4%.

Critical currents were calculated for different combinations of soil resistivity and ground impulse impedance. The high critical current values obtained for both the HV and MV circuits indicate the excellent lightning performance of the hybrid overhead line, even for the most challenging conditions considered in the analysis. It is unlikely that a subsequent stroke may cause a backflashover in either of the circuits.

Despite the significance of added insulation from the XLPE coverage of the spacer cable, the MV line shows good lightning performance even when a modest increase (50 kV) is considered in the withstand capability.

The main contributions of this research can be summarized as follows:

- a reliable model was developed and adopted for the representation of the towers of an actual hybrid overhead line both in scale model experiments and in simulations using the EMTP software. The model was validated through comparisons between measured and experimental results;
- a reliable model was developed to represent the HV insulators of an actual hybrid overhead line. The model consists of the parameters required for applying the Integration Method. The validation was confirmed based on comparisons of measured and calculated volt-time curves;
- a reliable model of a hybrid overhead line was implemented in the EMTP;
- a reduced-scale system was designed for experimental studies of lightning overvoltages on hybrid overhead lines. A section of four spans of an actual hybrid overhead line was implemented at the Scale Model Laboratory of the Institute of Energy and Environment of the University of São Paulo;
- measurements of currents and voltages were performed and comparisons were carried out between measured and calculated (EMTP) currents and voltages on this type of line for the first time. The deviations between the measured and calculated absolute values of the peak voltages indicated the suitability of the models used in both the EMTP simulations and the reduced scale system for investigating lightning surges in hybrid overhead lines;

- the influence of the most important parameters on the MV line overvoltages were investigated using validated models for all the system components;
- the critical currents (first and subsequent strokes) for the HV and MV circuits of the hybrid overhead line were estimated considering different conditions for the soil resistivity and ground impulse impedance.

Finally, the results obtained in this research have contributed to the CIGRE Working Group (WG) C4.67 (Lightning Protection of Hybrid Overhead Lines).

Looking ahead, to assess the general applicability of the results, future investigations will include experimental analyses using reduced-scale models with diverse configurations of hybrid overhead lines. Such analysis, which will also involve overvoltages caused by indirect lightning strokes, will include the low voltage line.

REFERENCES

ALTERNATIVE Transients Program. [s.d.]. Available at : <http://www.atpdesigner.de/network_calculation_and_protection_relays/downloads/index. Acesso em: 10 agosto 2023.

AMETANI, A.; KAWAMURA, T. A Method of a Lightning Surge Analysis Recommended in Japan Using EMTP. **IEEE Transactions on Power Delivery**, v. 20, n. 2, p. 867–875, abr. 2005.

ANCAJIMA, A. et al. Optimal selection of disruptive effect models parameters for the reproduction of MV insulators volt-time characteristics under standard and non standard lightning impulses. **2007 IEEE Lausanne Power Tech**. **Anais**...IEEE, jul. 2007.

ANDERSON, R. B.; ERIKSSON, A. J. Lightning parameters for engineering application. **Electra,** nº 69. 1980.

BABA, Y.; ISHII, M. Numerical electromagnetic field analysis on measuring methods of tower surge impedance. **IEEE Transactions on Power Delivery**, v. 14, n. 2, p. 630–635, abr. 1999.

BATISTA MORAES, L.; LOPES, G. P.; VIOLIN, A.; WANDERLEY NETO, E. T.; FERRAZ, G. M. F.; CAPELINI, R. M.; SALUSTIANO, R.; PIANTINI, A.; CAMPOS, J. M. Assessment of lightning overvoltages on lines with different voltages sharing the same structures. *In*: INTERNATIONAL SYMPOSIUM ON LIGHTNING PROTECTION, 14., 2017, Natal. **Proceedings**. SIPDA. IEEE, Oct. 2017a.

BATISTA MORAES, L.; LOPES, G. P.; VIOLIN, A.; PIANTINI, A.; WANDERLEY NETO, E. T.; FERRAZ, G. M. F.; CAPELINI, R. M.; SALUSTIANO, R.; CAMPOS, J. M. Assessment of the electromagnetic coupling between lines of different voltages sharing the same structures. **CIRED - Open Access Proceedings Journal**, v. 2017, n. 1, p. 531–534, 1, Oct. 2017b.

BATISTA MORAES, L.; PIANTINI, A.; SHIGIHARA, M.; BORGHETTI, A.; NAPOLITANO, F.; NUCCI, C. A.; TOSSANI, F. Analysis of Lightning Overvoltages on Overhead Hybrid Lines. *In:* INTERNATIONAL CONFERENCE ON LIGHTNING PROTECTION, 36., 2022, South Africa. **Proceedings**. ICLP. IEEE, 2 Oct. 2022.

BATISTA MORAES, L.; PIANTINI, A.; SHIGIHARA, M.; BORGHETTI, A.; NAPOLITANO, F.; NUCCI, C. A.; TOSSANI, F. Overvoltages Caused by Direct Lightning Strokes to a Hybrid Overhead Line. **Electrical Power Systems Research**, p. 1–22, 2024.

BATISTA MORAES, L.; PIANTINI, A.; SHIGIHARA, M. Insulator Models of a Hybrid Overhead Line. *In*: INTERNATIONAL SYMPOSIUM ON LIGHTNING PROTECTION, 17., 2023, Suzhou, China. **Proceedings**. SIPDA. Suzhou, China, 2023a.

BATISTA MORAES, L.; PIANTINI, A.; SHIGIHARA, M. Surge Impedance of a Hybrid Overhead Line Tower. *In*: INTERNATIONAL SYMPOSIUM ON LIGHTNING PROTECTION, 17., 2023, Suzhou, China. **Proceedings**. SIPDA. Suzhou, China, 2023b.

BORGHETTI, A.; FERRAZ, G. M.; NAPOLITANO, F.; NUCCI, C. A.; PIANTINI, A; TOSSANI, F. **Transient Response of a Double-Circuit Line to Direct and Indirect Lightning Strikes**. Saint Petersburg, Russia, April 2018a.

BORGHETTI, A.; FERRAZ, G. M.; NAPOLITANO, F.; NUCCI, C. A.; PIANTINI, A; TOSSANI, F**.** Lightning Protection of a Compact MV Power Line Sharing the same Poles of a HV Line**.** *In:* INTERNATIONAL CONFERENCE ON LIGHTNING PROTECTION, 34., 2018, Rzeszow, Poland. **Proceedings.** ICLP. IEEE, 2018b.

BORGHETTI, A.; NAPOLITANO, F.; NUCCI, C. A.; RIOS PENALOZA, J. D.; TOSSANI, F.; FERRAZ, G. M.; PIANTINI, A. Lightning-Originated Overvoltages in a Multi-Circuit HV-MV Line. *In*: 2019 IEEE MILAN POWER TECH. **Proceedings.** IEEE, June. 2019a.

BORGHETTI, A.; NAPOLITANO, F.; NUCCI, C. A.; PIANTINI, A; TOSSANI, F. Influence of ground unevenness and of line hybrid configuration on the lightning performance of medium-voltage overhead distribution systems. *In*: INTERNATIONAL SYMPOSIUM ON LIGHTNING PROTECTION, 15., 2019, São Paulo. **Proceedings**. SIPDA. São Paulo, October, 2019b.

BORGHETTI, A.; FERRAZ, G. M.; NAPOLITANO, F.; NUCCI, C. A.; PIANTINI, A; TOSSANI, F. Lightning protection of a multi-circuit HV-MV overhead line. **Electric Power Systems Research**, v. 180, p. 106119, March 2020.

CALDWELL, R.; DARVENIZA, M. Experimental and Analytical Studies of the Effect of Non-Standard Waveshapes on the Impulse Strength of External Insulation. **IEEE Transactions on Power Apparatus and Systems**, v. PAS-92, n. 4, p. 1420–1428, jul. 1973.

CHISHOLM, W.; CHOW, Y.; SRIVASTAVA, K. Travel Time of Transmission Towers. **IEEE Transactions on Power Apparatus and Systems**, v. PAS-104, n. 10, p. 2922–2928, Oct. 1985.

CHOWDHURI, P.; MISHRA, A. K.; MCCONNELL, B. W. Volt-time characteristics of short air gaps under nonstandard lightning voltage waves. **IEEE Transactions on Power Delivery**, v. 12, n. 1, p. 470–476, jan. 1997.

DARVENIZA, M. The generalized integration method for predicting impulse volt-time characteristics for non-standard wave shapes-a theoretical basis. **IEEE Transactions on Electrical Insulation**, v. 23, n. 3, p. 373–381, June 1988.

DATSIOS, Z. G.; MIKROPOULOS, P. N.; TSOVILIS, T. E. Effects of Lightning Channel Equivalent Impedance on Lightning Performance of Overhead Transmission Lines. **IEEE Transactions on Electromagnetic Compatibility**, v. 61, n. 3, p. 623–630, jun. 2019.

DUGAN, R. C.; SMITH, S. D. Low-voltage-side current-surge phenomena in single-phase distribution transformer systems. **IEEE Transactions on Power Delivery**, v. 3, n. 2, p. 637–647, abr. 1988.

GUSTAVSEN, B.; SEMLYEN, A. Simulation of transmission line transients using vector fitting and modal decomposition. **IEEE Transactions on Power Delivery**, v. 13, n. 2, p. 605–614, April 1998.

HEIDLER, F.; CVETIĆ, J. A class of analytical functions to study the lightning effects associated with the current front. **European Transactions on Electrical Power**, v. 12, n. 2, p. 141–150, March 2002.

HILEMAN, A. R. **Insulation Coordination for Power Systems**. [s.l.] CRC Press, 1999.

IEEE Guide for Improving the Lightning Performance of Electric Power Overhead Distribution Line. **IEEE Std 1410-2010**, p. 1-73, 21 Jan. 2011. Revision of IEEE Std 1410-2004

IEEE Guide for Improving the Lightning Performance of Transmission Lines. **IEEE Std 1243-1997**, p. 3-4, 26 jun. 1997.

ISHII, M.; KAWAMURA, T.; KOUNO, T.; OHSAKI, E.; SHIOKAWA, K.; MUROTANI, K.; HIGUCHI, T. Multistory transmission tower model for lightning surge analysis. **IEEE Transactions on Power Delivery**, v. 6, n. 3, p. 1327–1335, July 1991.

ISHII, M.; BABA, Y. Numerical electromagnetic field analysis of tower surge response. **IEEE Transactions on Power Delivery**, v. 12, n. 1, p. 483–488, 1997.

INTERNATIONAL ELECTROTECHNICAL COMISSION. **IEC 60060-1**: High-voltage test techniques-part 1: general definitions and test requirements. Ed. 3.0, Suisse, 2010.

LEAL, O. E. S.; DE CONTI, A. On the Influence of Dielectric-Coated Conductors on the Performance of Three-Phase Compact Distribution Lines Against Indirect Lightning Strikes. **IEEE Transactions on Electromagnetic Compatibility**, v. 63, n. 4, p. 1284–1289, ago. 2021.

MARQUES COSTA, E. C.; LOURENÇO, L. F. N. Evaluation of analytic formulations for surge impedance calculation of tall transmission towers. **International Journal of Electrical Power & Energy Systems**, v. 114, p. 105407, Jan. 2020.

MARTI, J. Accurate Modelling of Frequency-Dependent Transmission Lines in Electromagnetic Transient Simulations. **IEEE Transactions on Power Apparatus and Systems**, v. PAS-101, n. 1, p. 147–157, jan. 1982.

MORCHED, A.; GUSTAVSEN, B.; TARTIBI, M. A universal model for accurate calculation of electromagnetic transients on overhead lines and underground cables. **IEEE Transactions on Power Delivery**, v. 14, n. 3, p. 1032–1038, July 1999.

NOVITSKIY, A.; WESTERMANN, D. **Interaction of multi-circuit overhead transmission lines of different voltages located on the same pylons**. 2012 Electric Power Quality and Supply Reliability. IEEE, June 2012.

PGSTECH; POWERSYS. **Electromagnetic Transients Program (EMTP)**. 2023. Disponível em: <https://www.emtp.com>. Acesso em: 30 nov. 2023

PIANTINI, A. Lightning Overvoltages on Hybrid Overhead Lines (Invited Lecture). *In*: INTERNATIONAL SYMPOSIUM ON LIGHTNING PROTECTION, 17., 2023, Suzhou, China. **Proceedings**. SIPDA. Suzhou, China, 2023.

PIANTINI, A.; JANISZEWSKI, J. M. Application of scale models to the study of lightning transients in power transmission and distribution systems. *In*: Vernon Cooray; Farhad Rachidi; Marcos Rubinstein. (Org.). **Lightning Electromagnetics**. Volume 2: Electrical processes and effects (2nd Edition). 2ed.Londres: The Institution of Engineering and Technology, 2023, v. 2, p. 325-374.

PIANTINI, A.; JANISZEWSKI, J. M.; BORGHETTI, A.; NUCCI, C. A.; PAOLOME, M. A Scale Model for the Study of the LEMP Response of Complex Power Distribution Networks. **IEEE Transactions on Power Delivery**, v. 22, n. 1, p. 710–720, Jan. 2007.

PIANTINI, A.; BORGHETTI, A.; NUCCI, C. A. Lightning interaction with medium-voltage overhead power distribution systems. *In*: **Lightning Interaction with Power Systems -** Volume 2: Applications. [s.l.] Institution of Engineering and Technology, 2020. p. 113–172.

PROCEDURES for Estimating the Lightning Performance of Transmission Lines - New Aspects. [S.l.]: CIGRÉ, 2021. CIGRÉ W.G. C4.23. Technical Brochure 839.

RUGTHAICHAROENCHEEP, N.; THANSIPHRASERTH, W.; PHAYOMHOM, A. Comparison voltage across insulator strings of 69 kV and 24 kV lines due to lightning strokes to top pole and mid span. *In:* INTERNATIONAL UNIVERSITIES POWER ENGINEERING CONFERENCE, 47., Uxbridge, UK, 2012. **Proceedings.** UPEC. IEEE, September. 2012.

SHIGIHARA, M. et al. Evaluation of the performance of different methods for estimating the parameters of the disruptive effect model — Application to 15 kV insulators. **IEEE Transactions on Dielectrics and Electrical Insulation**, v. 23, n. 2, p. 1030–1037, abr. 2016.

SHIGIHARA, M. et al. Comparison of different procedures to predict the volt-time curves of 15 kV insulators. **Electric Power Systems Research**, v. 153, p. 82–87, dez. 2017.

SHIGIHARA, M.; PIANTINI, A.; BRAZ, C. P.; da SILVA, D. A.; KODAIRA, C. Y. Generation of Non-standard Lightning Impulse Unipolar Waveshapes. *In*: INTERNATIONAL CONFERENCE ON HIGH VOLTAGE ENGINEERING AND APPLICATION, Greece, 2018. **Proceedings**. ICHVE. IEEE, September. 2018.

TAKAHASHI, H. Confirmation of the error of Jordan's formula on tower surge impedance. **Transactions on Electrical and Electronic Engineering**, v. 114- B, p. 112–113, 1994.

VISACRO, S.; SILVEIRA, F. H. Lightning Performance of Transmission Lines: Requirements of Tower-Footing Electrodes Consisting of Long Counterpoise Wires. **IEEE Transactions on Power Delivery**, v. 31, n. 4, p. 1524–1532, August. 2016.

RAKOV, V.A.; BORGHETTI, A.; C. BOUQUEGNEAU, C; CHISHOLM, W.A.; COORAY, V.; CUMMINS, K.; DIENDORFER, G.; HEIDLER, F.; HUSSEIN, A.; ISHII, M.; NUCCI, C.A.; PIANTINI, A.; PINTO JR., O.; QIE, X.; RACHIDI, F.; SABA, M.M.F.; SHINDO, T.; SCHULZ, W.; THOTTAPPILLIL, R.; VISACRO, S.; ZISCHANK, W. CIGRE TB 549, **Lightning Parameters for Engineering Applications**, WG C4.407, 117 p., August 2013.

WAGNER, C. F.; HILEMAN, A. R. Lightning performance of transmission lines — III. **Electrical Engineering**, v. 79, n. 11, p. 903–903, November 1960.

WITZKE, R. L.; BLISS, T. J. Surge Protection of Cable-Connected Equipment. **Transactions of the American Institute of Electrical Engineers**, v. 69, n. 1, p. 527–542, jan. 1950.